AD NUMBER
AD868121
LIMITATION CHANGES
TO: **Approved for public release; distribution is unlimited.**
FROM: **Distribution authorized to U.S. Gov't. agencies and their contractors; Critical Technology; AUG 1968. Other requests shall be referred to Air Force Weapons Laboratory, ATTN: WLRET, Kirtland AFB, NM 87117. This document contains export-controlled technical data.**
AUTHORITY
AFWL ltr dtd 30 Nov 1971

RADIATION EFFECTS ON GALLIUM ARSENIDE DEVICES AND SCHOTTKY DIODES

Volume I

R. H. Schnurr

H. D. Southward

University of New Mexico

Albuquerque, New Mexico

Contract F29601-67-C-0051

TECHNICAL REPORT NO. AFWL-TR-68-31, Vol I

August 1968

AIR FORCE WEAPONS LABORATORY
Air Force Systems Command
Kirtland Air Force Base
New Mexico

AFWL-TR-68-31, Vol I

AIR FORCE WEAPONS LABORATORY
Air Force Systems Command
Kirtland Air Force Base
New Mexico

RADIATION EFFECTS ON GALLIUM ARSENIDE DEVICES AND SCHOTTKY DIODES

Volume I

R. H. Schnurr H. D. Southward
University of New Mexico
Albuquerque, New Mexico
Contract F29601-67-C-0051

TECHNICAL REPORT NO. AFWL-TR-68-31

FOREWORD

This report was prepared by the University of New Mexico, Albuquerque, New Mexico under Contract F29601-67-C-0051. The research was performed under Program Element 6.16.46.01H, Project 5710, Subtask 6.015, and was funded by the Defense Atomic Support Agency (DASA).

Inclusive dates of research were 15 February 1967 to 15 February 1968. The report was submitted 7 June 1968 by the AFWL Project Officer, Dr. J. S. Nichols (WLRE). Former Project Officers were Capt John Hubbard and Capt Gary Pritchard (WLRE).

The authors wish to express their sincere appreciation to Texas Instruments, Inc., for aid and cooperation in the pursuit of this research contract. We would like to specifically acknowledge the cooperation of Gary Hanson who coordinated our visits, of Hans Strack for helpful discussions involving GaAs, and of Shing Mao for helpful discussions involving the Gunn diodes.

The authors wish to acknowledge the assistance of MSgt Fred W. Fisher, SSgt Albert H. Hoffland, and SSgt Jon B. Toops for their operation of the flash X-ray machine.

This technical report has been reviewed and is approved.

J. S. NICHOLS
Project Officer

WILLIAM N. JACKOMIS
Major, USAF
Chief, Effects Branch

CLAUDE K. STAMBAUGH
Colonel, USAF
Chief, Research Division

ABSTRACT

(Distribution Limitation Statement No. 2)

The theory of operation of the Schottky barrier diode is reviewed, and complications caused by a more accurate space-charge formulation are discussed. Consideration is given to image effects, tunneling, interfacial dielectric layers, surface states, and minority carrier current.

The interaction of ionizing radiation with semiconducting materials is reviewed, as is the behavior of a Schottky barrier diode in an ionizing radiation environment. The resultant model for the Schottky barrier diode is analogous to a p-n diode with a very high dopant concentration on one side.

Tests were performed upon gallium arsenide (GaAs) and silicon Schottky barrier diodes, using a 2-Mev flash X-ray machine. The GaAs Schottky diodes were tested while functioning as an X-band detector and mixer. No permanent change was observed in the voltage-current or capacitance-voltage characteristics, or in the noise figure of the diodes after irradiation. Diodes fabricated from both types of material were also tested in a more conventional DC bias circuit.

Both types of diode were exposed to a mixed neutron gamma pulse at the Sandia Pulsed Reactor II. Neutron fluences up to 5×10^{14} nvt and gamma dose rates up to 10^{9} rad/sec were obtained. The diodes showed very minor changes in voltage current characteristics for a total neutron fluence up to 1.2×10^{15} nvt.

This page intentionally left blank.

CONTENTS

LIST OF FIGURES

List of Figures (continued)

LIST OF SYMBOLS

A	area of diode junction, meters^2
C	capacitance of diode junctions, farads
D_n	diffusion constant for electrons, meters^2/second
D_p	diffusion constant for holes, meters^2/second
E	electric field, volts/meter
E_B	energy on top of potential barrier, electron volts
E_C	energy of conduction band, electron volts
E_f	energy of Fermi level, electron volts
E_g	width of forbidden band gap, electron volts
E_i	energy of center of forbidden band gap, electron volts
E_{iB}	energy of center of forbidden band gap in bulk material, electron volts
E_{io}	electric field across insulator, volts/meter
E_m	maximum electric field, volts/meter
E_{mo}	maximum electric field with zero applied bias, volts/meter
E_R	energy necessary to produce one electron-hole pair by radiation, electron volts
E_v	energy of valence band, electron volts
E_x	energy associated with particle of velocity v_x, electron volts
L_n	diffusion length for electron, meters
L_p	diffusion length for holes, meters
N_A	acceptor density, meter^{-3}
N_D	donor density, meters^{-3}

N_S	surface state density, [electron volts-meter^2]$^{-1}$
Q_m	charge in metal, Coulombs
Q_{sc}	charge in space charge region, Coulombs
Q_{ss}	charge in surface states, Coulombs
R	dose rate, rads/second
T	temperature, ^oK
V	applied bias voltage, volts
V_{BO}	barrier height caused by surface states, volts
V_D	barrier height, volts
V_{DO}	barrier height with zero applied bias, volts
V_i	voltage across insulator, volts
V_{io}	voltage across insulator with zero applied bias, volts
g	electron-hole pair generation rate, meters^{-3}
j	net current density, amperes/meter^2
j_+	positive current density, amperes/meter^2
j_-	negative current density, amperes/meter^2
j_n	electon current density, amperes/meter^2
j_o	reverse saturation current density, amperes/meter^2
j_p	hole current density, amperes/meter^2
j_x	component of current density in x direction, amperes/meter^2
k	Boltzmann constant, 1.38×10^{-23} joules/^oK
ℓ	depletion width, meters
ℓ_o	depletion width with zero applied bias, meters
m*	effective mass, kilograms

List of Symbols (cont'd)

n	electron concentration, meters^{-3}
n_i	electron concentration for intrinsic material, meters^{-3}
n_o	thermal equilibrium density of electrons in the conduction band, meters^{-3}
n_x	density of mobile electrons in conduction band with a velocity in the x direction, meters^{-3}
p	hole concentration, meters^{-3}
q	electronic charge, 1.6×10^{-19} Coulombs
v_x	x component of velocity, meters/second
w	width of insulator, meters
x	distance into semiconductor measured from surface, meters
x_m	location of potential barrier maximum, meters
ϵ_i	dielectric constant of insulator, farads/meter
ϵ_s	dielectric constant of semiconductor, farads/meter
μ_n	electron mobility, meters/volt-second
μ_p	hole mobility, meters/volt-second
ρ	density of material, kilograms/meter^3
$\rho(x)$	volume charge density, Coulombs/meter^3
τ_n	minority carrier lifetime for electrons, seconds
τ_p	minority carrier lifetime for holes, seconds
φ_m	work function of metal, electron volts
φ_s	work function of semiconductor, electron volts
χ_i	electron affinity for insulator, electron volts
χ_s	electron affinity for semiconductor, electron volts

List of Symbols (cont'd)

ψ	potential distribution, volts
$\Delta\psi_m$	change in maximum potential, volts
ψ_{sc}	potential distribution in semiconductor, volts
ψ_{sco}	potential distribution in semiconductor with zero applied bias, volts

This page intentionally left blank.

SECTION I

INTRODUCTION

Metal semiconductor junctions have been studied for many years (Ref. 1). The point-contact rectifier has been used since the earliest days of radio. The most satisfactory early rectifiers, based upon lead sulphide, could not be reproduced with precise uniformity. Other rectifiers were made from germanium and silicon pellets which were ground smooth and polished. The junction was formed by touching the semiconductor with a thin metal wire. The wire tip was moved until a sensitive spot was found. Mechanical tapping of the whisker mount improved the rectification and stability of the device. Mechanical forming of point-contact diodes is still used.

The development of a workable theory for the metal semiconductor junction had to wait for the development of the band theory of solids. Theories explaining the behavior of the metal semiconductor junctions were formulated by Schottky and Mott. These models are the basis for the more elaborate theories of today. As technology was able to provide more uniformly reproducible rectifiers, the first theories have been modified and refined to explain additional experimental data.

Modern technology is now able to form deposited metal contacts the same size as the point of the wire in the point-contact diodes. This capability is reflected by the appearance of metal semiconductor or Schottky barrier diodes on the commercial market. The Schottky barrier diodes are stronger mechanically than point-contact diodes. The junction of the Schottky barrier diodes is formed under controlled conditions and is therefore more precisely reproducible.

Schottky barrier diodes are used as parametric amplifiers, harmonic generators, multipliers, mixers, high-speed switches, and voltage-tuned or modulated oscillators. Because of their versatility, Schottky barrier diodes can be used in many sophisticated military and space systems.

Military and space systems may be exposed to environments containing high radiation levels. Consequently, the circuit designer must know the effect of radiation upon the components he uses in order to minimize undesirable radiation-induced transients or changes in the system.

Information is available which describes in detail the effect of radiation upon p-n junction diodes, transistors, integrated circuits, and other active and passive components. This paper has been written to characterize the Schottky barrier diode in a radiation environment.

The simple theory of a metal semiconductor junction as proposed by Schottky is developed in the first part of Section II. A more accurate formulation for the space charge is discussed. Considerations of image effects, tunneling, interfacial dielectric layers, surface states, and minority carrier current are also included.

Section III begins with a discussion of the interaction of ionizing radiation with matter. The interaction processes discussed are photoelectric, Compton, pair production and photodisintegration. The effect of ionizing radiation upon semiconductors is then considered. Section III is concluded with a discussion of the effect of ionizing radiation on Schottky barrier diodes.

The Schottky barrier diodes were irradiated at the Kirtland Air Force Base 2-Mev flash X-ray machine. The results of these tests are reported in Section IV. The photocurrent was measured and compared with the theory developed in Section III. The diodes were also tested operationally as detectors and mixers.

Further testing is reported on in Appendix III. The Schottky barrier diodes were irradiated at the Sandia Pulsed Reactor II. Transient annealing and permanent degradation of the diodes were observed.

SECTION II

SCHOTTKY BAPRIER THEORY

To provide an insight into the theory of a Schottky barrier, the simple model proposed by Schottky is discussed. Next, complications are considered that arise from more nearly exact space configurations, image force, quantum-mechanical tunneling, surface states, interfacial dielectric layers, and minority carrier currents.

Elementary Schottky Barrier Theory

The simplest model for the rectifying metal semiconductor junction is that developed by Schottky. The model is best explained by use of the band model of solids showing the band structure in the metal and semiconductor both before and after contact.

In figure 1a, a metal semiconductor junction is shown before contact. φ_m is the work function of the metal, φ_s is the work function of the semiconductor, and χ_s is called the electron affinity of the semiconductor. There is an energy difference of $\varphi_m - \varphi_s$ between the Fermi levels in the metal and those in the semiconductor.

When the two materials are brought into intimate contact, thermal equilibrium requires that their Fermi levels coincide. It may be reasonably assumed that both materials were originally uncharged and that both materials

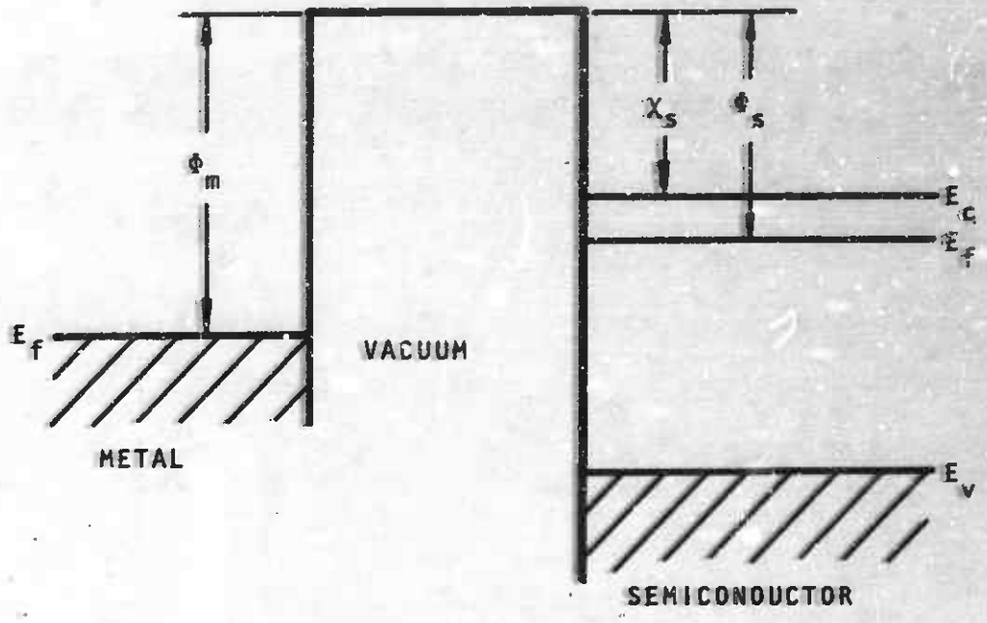

a) Before contact

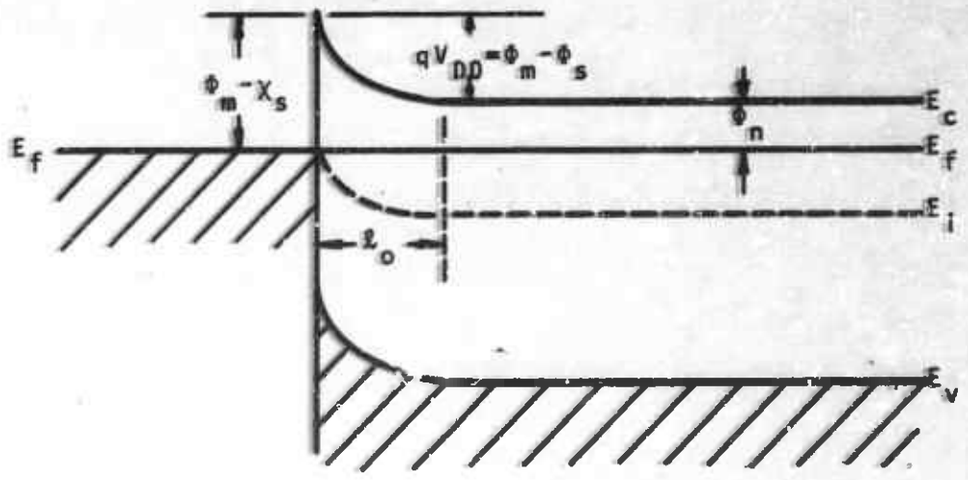

b) After contact and with thermal equilibrium

Figure 1. Metal Semiconductor Junction

will exhibit their bulk properties at some distance from their common interface. The contact potential, caused by the difference in Fermi-level energies, must, therefore, appear across the junction. The contact potential, defined by

$$V_{DO} = \frac{1}{q} (\varphi_m - \varphi_s) , \qquad (1)$$

will cause a redistribution of charge at the junction.

Schottky proposed that a double layer be formed at the junction. At the instant a junction is established, electrons will flow from the semiconductor into the metal until the contact potential is neutralized by the charge layer. A negative surface charge is developed upon the metal. An opposite and equal charge must be built up in the semiconductor, but in the absence of surface states the positive charge must be distributed over fixed ionized atoms in the semiconductor forming a space charge layer. The resultant charge distribution after contact is illustrated in figure 1b.

The customary treatment of the problem is to assume a uniformly doped semiconductor with the impurity donor density, N_D. Further, assume the semiconductor is completely depleted of electrons for a distance, ℓ_o, from the junction. The depletion width, ℓ_o, can be determined by solving Poisson's equation

$$\frac{d^2\psi}{dx^2} = - \frac{\rho(x)}{\epsilon_s} \qquad (2)$$

where

ψ = potential distribution

x = distance into semiconductor from the surface

$\rho(x)$ = space charge density

ϵ_s = dielectric constant of the semiconductor

From the assumptions we can write,

$$\rho = + q N_D \qquad 0 \leq x \leq \ell_o$$

$$\rho = 0 \qquad \ell_o < x \qquad (3)$$

The boundary conditions for equation 2 are $\frac{d\psi}{dx} = 0$ at $x = \ell_o$, and $\psi = 0$ at $x = \ell_o$.

$$\ell_o = \left[\frac{2\epsilon_s V_{DO}}{qN_D}\right]^{1/2} \qquad (4)$$

$$\psi_{sco} = - \frac{qN_D}{2\epsilon_s} [x - \ell_o]^2 \qquad 0 \leq x \leq \ell_o \qquad (5)$$

and

$$E_{mo} = - \left[\frac{2qN_D V_{DO}}{\epsilon_s}\right]^{1/2} = - \frac{2V_{DO}}{\ell_o} \qquad (6)$$

We define ψ_{sco} as the potential distribution in the semiconductor with no bias applied and E_{mo} as the maximum electric field with no bias applied.

Behavior with Applied Bias

The effect of applied bias is easily incorporated into equations 4, 5, and 6. Suppose a bias voltage is applied in some manner to a Schottky barrier device so that the n-type semiconductor is made positive with respect to the metal. The total applied voltage must be shared by voltage drops across the ohmic contacts, the bulk material, and the barrier region. For small currents, the voltage drops across the ohmic contacts, and bulk material can be neglected. The voltage drop across the barrier region will cause a change in the barrier as illustrated in figure 2. Equations 4, 5, and 6 can be generalized to give the variations in depletion width, potential, and electric field with an applied bias:

$$\ell = \left[\frac{2\epsilon_s(V_{DO} + V)}{qN_D}\right]^{1/2} \tag{7}$$

$$\psi_{-c} = -\frac{qN_D}{2\epsilon_s}[x - \ell]^2 \tag{8}$$

$$E_m = -\left[\frac{2qN_D(V_{DO} + V)}{\epsilon_s}\right]^{1/2} = -\frac{2(V_{DO} + V)}{\ell} \tag{9}$$

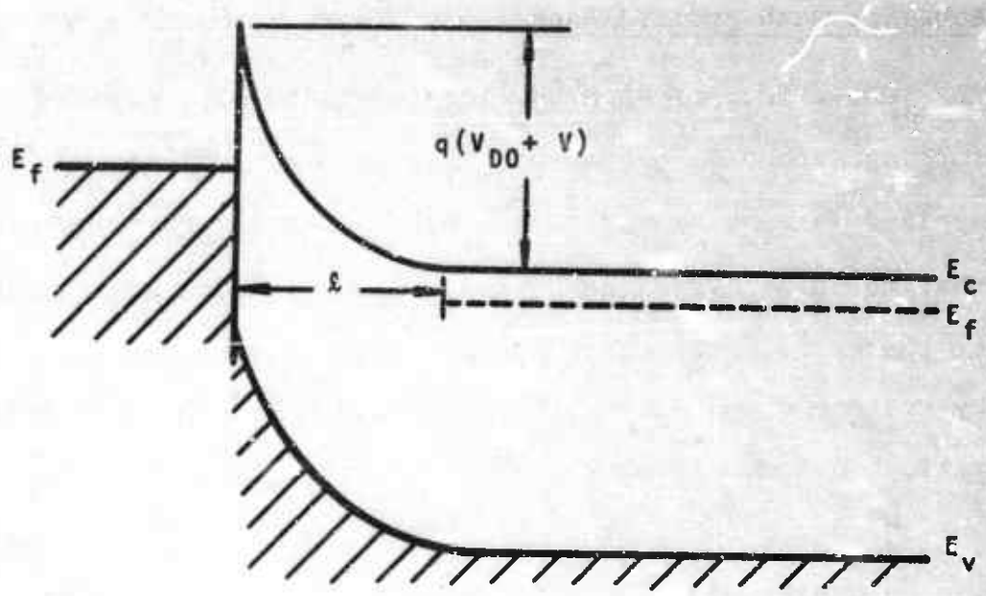

Figure 2. Metal Semiconductor Junction with Applied Reverse-Bias Voltage V

Junction Capacitance

A charge, Q_{sc}, is stored in the depletion region. Its magnitude is dependent upon the volume charge density, $\rho(x)$, and the width of the depletion region. That is,

$$Q_{sc} = \rho(x)\,\ell$$

$$= qN_D\ell = [2\epsilon_s N_D q(V_{DO} + V)]^{1/2} \qquad (10)$$

The total charge is dependent upon applied voltage. The junction can therefore be considered to be a capacitor. The capacitance per unit function area is given by

$$C(V) = \frac{dQ_{sc}}{dV} = \left[\frac{\epsilon_s N_D q}{2(V_{DO} + V)}\right]^{1/2} = \frac{\epsilon_s}{\ell} \qquad (11)$$

The capacitance as a function of voltage may be experimentally obtained, using a small signal AC capacitance bridge. By rearranging equation 11 we can observe that a plot of $1/C^2$ vs V will allow determination of N_D and V_{DO}.

$$1/C^2 = \frac{2}{\epsilon_s N_D q} (V_{DO} + V) \qquad (12)$$

$$\frac{d[1/C]^2}{dV} = \frac{2}{\epsilon_s N_D q} \qquad (13)$$

From equation 12 we see that when $1/C^2$ is zero, $V = -V_{DO}$. Equation 13 gives the slope of the $1/C^2$ curve. If the dielectric constant of the semiconductor is known, the slope can be used to determine N_D.

Current-Voltage Characteristics

There are two theories that describe current flow in a Schottky barrier junction (Ref. 1). The diode or thermionic emission theory assumes that the mean free path of electrons in the semiconductor conduction band is longer than the width of the depletion region, ℓ_o. The above assumption implies that collisions within the barrier are rare and that current flow in the junction is by thermionic emission

over the barrier. In contrast, the diffusion theory assumes that many collisions occur in the barrier and that carriers are affected by both diffusion and electric forces.

Thermionic Emission -- To derive the current flow in the junction we must first determine the distribution of electrons with a velocity toward the barrier as a function of energy. This function can be obtained from the classical velocity distribution of electrons (Ref. 2). The same expression can be derived, starting with the Fermi distribution function as shown in Appendix I.

$$dn_x = N_D \left(\frac{m^*}{2\pi kT} \right)^{1/2} e^{-\frac{m^* v_x^2}{2kT}} dv_x \qquad (4)$$

$$dn_x = \frac{1}{2} N_D \left(\frac{1}{\pi kT} \right)^{1/2} (E_x)^{-1/2} e^{-E_x/kT} dE_x$$

where

n_x = density of electrons with velocity in the x direction between v_x and $v_x + dv_x$

m^* = effective mass

v_x = x component of velocity

k = Boltzmann constant

T = temperature

E_x = energy associated with electron of velocity v_x

The current density, j_x, is then obtained by multiplying the electron density by the electron velocity and an electronic charge and integrating over all energies higher than the barrier.

$$j_x = \int - q\, v_x dn_x$$

$$j_x = \int_{E_B}^{\infty} - q\, N_D \left[\frac{1}{2\pi\, m^* kT}\right]^{1/2} e^{-E/kT}\, dE_x \qquad (15)$$

$$j = -q\, N_D \left[\frac{kT}{2\pi\, m^*}\right]^{1/2} e^{-E_B/kT} \qquad (16)$$

For an electron in the bottom of the conduction band of the semiconductor, the barrier will appear to be $E_B = qV_D$ electron volts high, where $V_D = V_{DO} + V$. Electrons flowing from right to left in figure 2 contribute to a conventional current flow from left to right. Therefore, an electron in the semiconductor that crosses the barrier will contribute to the positive component of the current density j_+.

$$j_+ = + qN_D \left[\frac{kT}{2\pi\, m^*}\right]^{-1/2} e^{-qV_D/kT} \qquad (17)$$

When zero bias is applied, no net current flows across the junction. Therefore, there is a negative component of current density, j_-, with electrons flowing from the metal to the semiconductor such that the net current flow is zero. Therefore

$$j_- = - qN_D \left[\frac{kT}{2\pi\, m^*}\right]^{1/2} e^{-qV_{DO}/kT} \qquad (18)$$

The total current density is the sum of its two components.

$$j = j_+ + j_-$$

$$= qN_D \left[\frac{kT}{2\pi m^*}\right]^{1/2} e^{-qV_{DO}/kT} \left[e^{-qV/kT} - 1\right] \qquad (19)$$

which can be written

$$j = j_o \left[e^{-qV/kT} - 1\right] \qquad (20)$$

where

$$j_o = qN_D \left[\frac{kT}{2\pi m^*}\right]^{1/2} e^{-qV_{DO}/kT} \qquad (21)$$

Under reverse bias, i.e., $V > 0$, j will rapidly approach j_o, the saturation current density. For forward bias, $V > \frac{3kT}{q}$, equation 20 may be written

$$\ln j = \ln j_o - \frac{qV}{kT} \qquad (22)$$

A plot of $\ln j$ vs. V should have a slope of $-\frac{q}{kT}$ for all barriers and temperatures.

Further observation of equation 20 will show that the asymmetrical properties of the diode do not depend upon either the barrier height or width.

Diffusion Theory -- Diffusion theory is similar to the thermionic theory except that collisions are allowed in the barrier region. Current flow will depend upon local electric fields and carrier distribution. The carriers will move by two mechanisms. These are drift caused by the electric

field and diffusion caused by the gradient in mobile carriers. The two mechanisms are related to the current density by the following equation:

$$j = q\mu_n E(x)\, n(x) + qD_n \frac{dn}{dx} \qquad (23)$$

where

μ_n = electron mobility

D_n = electron diffusion constant

n = density of electrons in conduction band

E = electric field

If the Einstein relation,

$$\mu_n = \frac{q}{kT} D_n$$

holds and

$$n_o = N_D\, e^{-qV_D/kT}$$

the equation can be solved as shown in Van der Ziel (Ref. 2) to give

$$j = qN_D\mu_n \left[\frac{2qN_D(V_D + V)}{\epsilon_s}\right]^{1/2} e^{-qV_D/kT} \left(e^{-qV/kT} - 1\right) \qquad (24)$$

The assumption that the Einstein relations hold is in this case questionable. μ_n is a constant for electric-field strength of 10^{+4} volts/meter or less (Ref. 3). The

maximum electric field for a lightly doped ($N_D = 10^{22} meter^{-3}$) silicon Schottky barrier diode is approximately 2×10^6 volts/meter. Therefore, in the depletion region μ_n is a function of the electric field.

Experiments on Schottky barrier diodes have shown that the conduction is probably by the thermionic mechanism. Therefore, nothing further will be said at this time about diffusion of majority carriers.

The Effect of a More Accurate Space Charge Formulation

For the elementary solution, the space charge density was assumed equal to the donor density multiplied by the charge of an electron as shown in equation 3. A more nearly exact form for the space charge density assuming no traps is

$$\rho(x) = q\,(N_D - N_A + p - n) \qquad (25)$$

where

N_D = donor density

N_A = acceptor density

p = free hole density

n = free electron density

The assumptions necessary to reduce equation 25 to equation 3 are as follows:

1. The semiconductor is an n-type material where $N_D >> N_A$ and $n >> p$.

2. The barrier is completely depleted of free carriers.

$$n = o \qquad o \leq x \leq \ell$$

$$n = N_D \qquad x > \ell$$

If the simplifying assumptions are not made, Poisson's equation becomes

$$\frac{\partial^2 \psi}{\partial x^2} = - \frac{q}{\epsilon_s} (N_D - N_A + p - n) \tag{26}$$

Assuming complete ionization of substitutional impurities in the bulk material far from the surface, charge neutrality requires that

$$N_D - N_A = n - p \tag{27}$$

In the bulk material the free carrier densities can be written

$$n = n_i \, e^{-(E_i - E_f)/kT} \tag{28}$$

and

$$p = n_i \, e^{-(E_f - E_i)/kT} \tag{29}$$

Combining equations 27, 28, and 29, we get

$$N_D - N_A = n_i \left(e^{(E_f - E_i)/kT} - e^{-(E_f - E_i)/kT} \right)$$

$$= 2n_i \sinh \left(\frac{E_f - E_i}{kT} \right) \tag{30}$$

We can see in figure 1b that E_i varies in the region $o \leq x \leq \ell$. To aid in solution of Poisson's equation, let us define the following potentials which are related to the Fermi level

$$\xi_B = \frac{1}{q} (E_f - E_{iB}) \tag{31}$$

where

E_{iB} = the center of the band gap in the bulk material

and

$$\xi = \frac{1}{q} (E_f - E_i) \tag{32}$$

where

E_i = the center of the band gap, which is a function of ψ.

Now we may write

$$N_D - N_A = 2n_i \sinh \left(\frac{q\xi_B}{kT}\right) \tag{33}$$

$$n - p = 2n_i \sinh \left(\frac{q\xi}{kT}\right) \tag{34}$$

Poisson's equation can therefore be rewritten in the form

$$\frac{\partial^2 \xi}{\partial x^2} = - \frac{2qn_i}{\epsilon_s} \left[\sinh \left(\frac{q\xi_B}{kT}\right) - \sinh \left(\frac{q\xi}{kT}\right)\right] \tag{35}$$

Multiplying Equation 35 by $\frac{d\xi}{dx}$ and integrating from the bulk region to a point in the depletion region of the semiconductor, one obtains

$$\int_0^{\frac{d\xi}{dx}} \frac{1}{2}\frac{d}{dx}\left(\frac{d\xi}{dx}\right)^2 = -\frac{2qn_i}{\epsilon_s}\int_{\xi_B}^{\xi}\left[\sinh\left(\frac{q\xi_B}{kT}\right) - \sinh\left(\frac{q\xi}{kT}\right)\right]d\xi$$

This equation results in

$$\frac{d\xi}{dx} = \sqrt{\frac{4n_i kT}{\epsilon_s}}\left[\left(\frac{q\xi_B}{kT} - \frac{q\xi}{kT}\right)\sinh\frac{q\xi_B}{kT} - \left(\text{oosh}\,\frac{q\xi_B}{kT} - \cosh\frac{q\xi}{kT}\right)\right]^{\frac{1}{2}} \quad (36)$$

This expression is the negative of the electric field in the barrier region. The potential distribution can only be found by the solution of the nonlinear differential equation (i.e., equation 36). The total charge and the change in mobile carriers can be determined by other techniques (Ref. 4).

Another approximation to the charge distribution is that of Schwartz and Walsh (Ref. 5). They assume that

$$N_D >> N_A \quad (37)$$

$$n = N_D e^{-q(\xi-\xi_B-V)/kT} \quad (38)$$

$$p = N_D e^{q(\xi-E_g/q+\xi_B)/kT} \quad (39)$$

These assumptions result in Poisson's equation of the form,

$$\frac{d^2\xi}{dx^2} = \frac{q}{\epsilon_s} N_D\left[1 + e^{q(\xi-E_g/q+\xi_B)/kT} - e^{-q(\xi-\xi_B-V)/kT}\right] \quad (40)$$

The solution to equation 40 yields a result that is tractable only by numerical techniques.

Other interesting models for charge distribution have been considered. For another example see Seiwatz and Green (Ref. 6).

The Effect of Image Force on Barrier Shape

As an electron in the semiconductor approaches the metal interface, it will be subjected to a force caused by its image in the metal. This force is

$$F = \frac{q^2}{4\pi\epsilon_s (2x)^2} \tag{41}$$

By integration of the force the electric potential is

$$\psi(x) = + \frac{q}{16\pi\epsilon_s x} \tag{42}$$

Since the force is an attractive one, this potential reduces the potential barrier at the interface. The total potential can now be written

$$\psi(x) = - \frac{qN_D}{2\epsilon_s} (x - \ell)^2 + \frac{q}{16\pi\epsilon_s x} \tag{43}$$

The change in barrier height can be determined by solving equation 43 for its maximum and subtracting the result from

equation 8 evaluated at x = 0. The potential caused by image effects falls off rapidly with distance. Therefore we can assume $x \ll \ell$.

$$x_m = \frac{1}{4}\left[\frac{q}{2\pi^2 N_D \epsilon_s (V_{DO} + V)}\right]^{1/4} \tag{44}$$

$$\Delta\psi_m = \frac{1}{2}\left[\frac{q^3 N_D}{8\epsilon_s^3 \pi^2}(V_{DO} + V)\right]^{1/4} \tag{45}$$

where

x_m = the value of x for maximum potential

$\Delta\psi_m$ = the change in maximum values of potential

The barrier height as seen from the semiconductor is now

$$\text{Barrier height} = V_{DO} + V - \Delta\psi_m \tag{46}$$

as shown in figure 3. If we let

$$\Delta\psi_m = \Delta\psi_m(V) + \Delta\psi_m(V_{DO}) \tag{47}$$

then the current equation 20 becomes

$$j = j_o\, e^{q\Delta\psi_m(V_{DO})/kT}\left[e^{-q[V-\Delta\psi_m(V)]/kT} - 1\right] \tag{48}$$

From equation 48, we can see that the inclusion of image effects causes an increase in reverse leakage current.

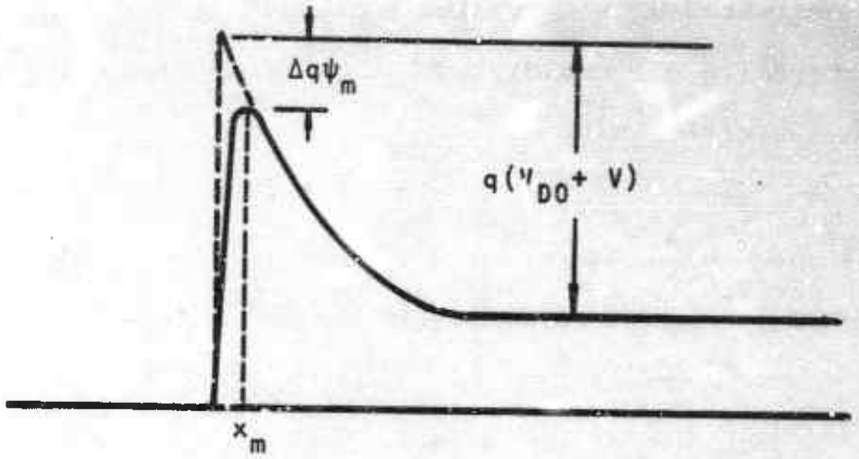

Figure 3. Distortion of the Barrier Caused by Image Effects

The Effect of Tunneling

Some of the early workers felt that the metal-semiconductor diode could be explained by quantum-mechanical tunneling of electrons through the potential barrier (Ref. 1). As more became known about the physical properties of the barrier these early concepts were shown to be questionable. Cowley (Ref. 7) and Crowell and Sze (Refs. 8 and 9) have calculated transmission coefficients for various idealized barriers, using computer-aided solutions. These solutions show the effect on the current to be the same as that of a small voltage-dependent barrier lowering.

On the other hand, Padovani and Stratton (Ref 10) have developed a model for the Schottky barrier which has a temperature-dependent conduction mechanism. At low temperatures, the dominant conduction mechanism is field emission with the center of the transmitted electron energy distribution equal to the upper filled states in the conduction band. For higher temperatures, the conduction mechanism becomes a combination thermionic-field emission with the center of the energy distribution somewhere above the low-temperature case but below the top of the barrier. Finally, at high temperatures the conduction mechanism becomes thermionic emission as predicted by the more elementary theories.

Padovani and Stratton's reported data show good agreement with the theory for Shottky barriers made from Au-GaAs with an impurity concentration of 10^{22} atoms/meter^3 or greater. Experiments performed with lightly doped GaAs did not agree with the theory.

The Effect of Interfacial Layers

The model for the Schottky barriers used so far has assumed an intimate contact between the metal and the semiconductor. The problem of creating a clean surface is widely recognized. Most semiconductor surfaces will

readily combine with oxygen to form an oxide. It is very probable that the contact between the metal and the semiconductor is not intimate. We will therefore investigate the effect of an interfacial insulating layer on the characteristics of the Schottky barrier diode. Goodman (Ref. 11) has shown that barrier capacitance is changed by the presence of an interfacial layer.

Figure 4a shows a band diagram of a metal-interfacial layer-semiconductor junction before contact and before thermal equilibrium is achieved. A calculation by Cowley (Ref. 7) shows that there is negligible bending of the bands in the insulator due to surface charges. We will therefore assume straight bands with a slope determined by applied electric field for the insulator. The resultant junction in thermal equilibrium is shown in figures 4b and 4c.

As shown in equation 10, the surface charge in the semiconductor with no bias applied is

$$Q_{sc} = [2q\epsilon_s N_D V_{DO}]^{1/2} \tag{10}$$

Figure 4c shows that

$$\varphi_m - \chi_i = + qV_{iO} + (\chi_s - \chi_i) + qV_{DO} + (\varphi_s - \chi_s)$$

$$\varphi_m - \varphi_s = + q(V_{iO} + V_{DO}) \tag{49}$$

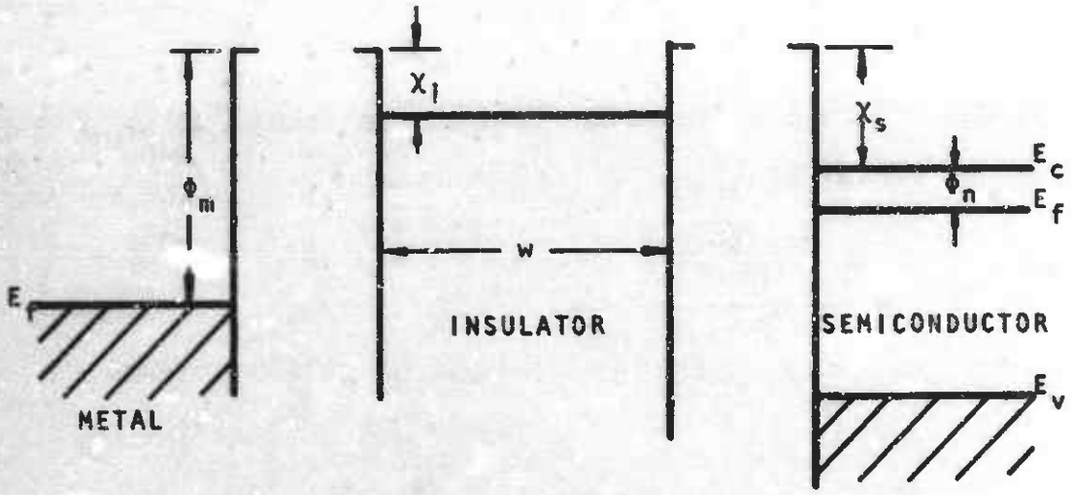

a) Before contact, not in thermal equilibrium

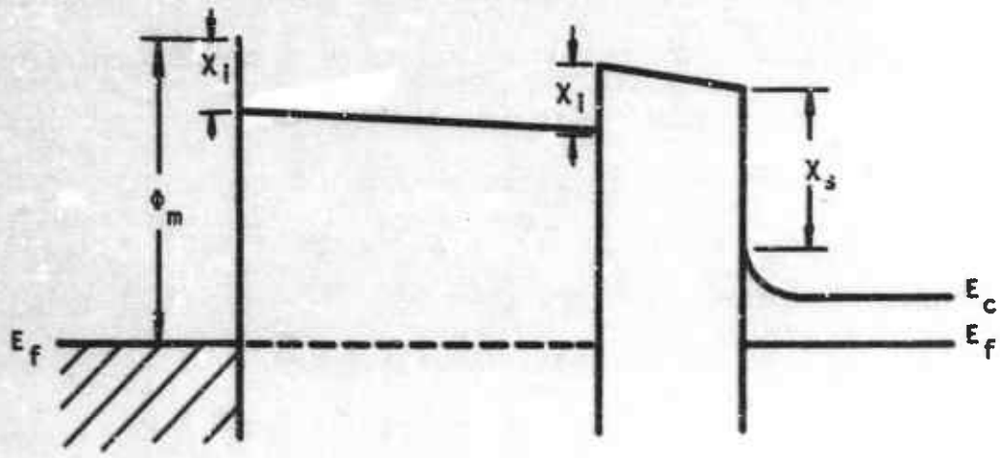

b) Before contact, in thermal equilibrium

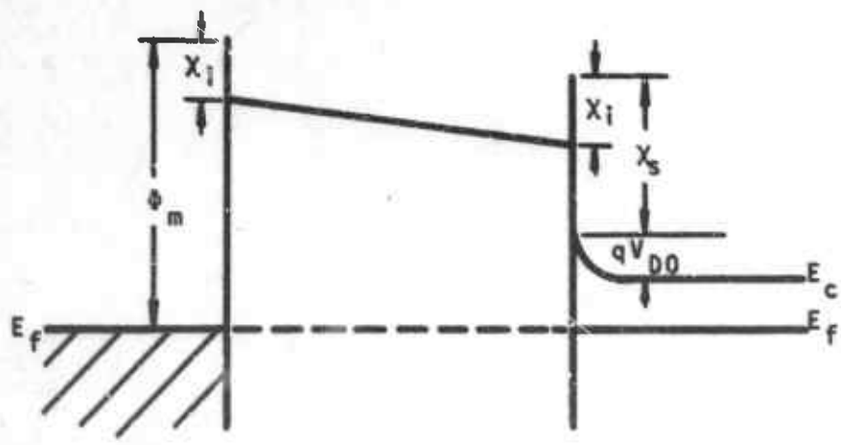

c) After contact, in thermal equilibrium

Figure 4. Metal-Insulator-Semiconductor Junction

By Gauss' law the electric field in the insulator, E_{iO}, can be shown to be

$$E_{iO} = \frac{Q_{sc}}{\epsilon_i} = \frac{[2\epsilon_s qN_D V_{DO}]^{1/2}}{\epsilon_i} \qquad (50)$$

where

ϵ_i = the dielectric constant in the insulator.

The electric field across the insulator can also be determined from the potential, V_{iO}, across the insulator.

$$E_{iO} = \frac{V_{iO}}{W} = \frac{\frac{1}{q}(\varphi_m - \varphi_s) - V_{DO}}{W} \qquad (51)$$

where

W = width of the insulating region.

Equating equations 50 and 51 and defining the constant

$$V_1 = \frac{W^2 \epsilon_s qN_D}{\epsilon_i^2} \qquad (52)$$

we get

$$V_{DO} = \frac{(\varphi_m - \varphi_s)}{q} + V_1 - \sqrt{V_1^2 + 2V_1\left(\frac{\varphi_m - \varphi_s}{q}\right)} \qquad (53)$$

Note that V_{DO} in equation 53 includes the effect of an insulator between the metal and the semiconductor. Therefore, it is not the same as that defined by equation 1.

As the interfacial layer width, W, decreases toward zero, equation 53 approaches equation 1, the original definition of V_{DO}. The potential across the interfacial layer is

$$V_{iO} = + \frac{1}{q} (\varphi_m - \varphi_s) - V_{DO}$$

$$V_{iO} = -V_1 + \sqrt{V_1^2 + 2V_1\left(\frac{\varphi_m - \varphi_s}{q}\right)} \qquad (54)$$

In the presence of an applied potential, equation 49 becomes

$$\varphi_m - \varphi_s + V = q(V_i + V_D) \qquad (55)$$

Following calculations similar to those in the zero bias case we can show that

$$V_D = \frac{\varphi_m - \varphi_s}{q} + V_1 + V - \sqrt{V_1^2 + 2V_1\left(V + \frac{\varphi_m - \varphi_s}{q}\right)} \qquad (56)$$

The potential across the interfacial region is given by

$$V_i = \frac{1}{q}(\varphi_m - \varphi_s) + V - V_D$$

$$V_i = -V_1 + \sqrt{V_1^2 + 2V_1\left(V + \frac{\varphi_m - \varphi_s}{q}\right)} \qquad (57)$$

where V_1 is given by equation 52.

The capacitance of the junction can be determined from

$$C = \frac{\partial Q_{sc}}{\partial V} \qquad (58)$$

and

$$Q_{sc} = \frac{\epsilon_i V_i}{W} = \frac{\epsilon_i}{W}\left[-V_1 + \sqrt{V_1^2 + 2V_1\left(V + \frac{\varphi_m - \varphi_s}{q}\right)}\right] \qquad (59)$$

By applying equation 58 to equation 59 and using equation 52 we obtain

$$C = \left[\frac{q\epsilon_s N_D}{2V + 2\frac{\varphi_m - \varphi_s}{q} + V_1}\right]^{1/2} \qquad (60)$$

which is similar to equation 11 with the addition of the term in V_1.

The customary presentation of capacitance information takes the form of a plot of $1/C^2$ vs V, which in this case is given by

$$\frac{1}{C^2} = \frac{2}{q\epsilon_s N_D}\left[V + \frac{\Phi_m - \Phi_s}{q} + \frac{V_1}{2}\right] \qquad (61)$$

The V axis intercept occurs at

$$V = -\frac{\Phi_m - \Phi_s}{q} - \frac{V_1}{2} \qquad (62)$$

The interface effects a shift of the intercept toward the -V or forward bias direction. The slope of the $1/C^2$ curve, however, remains unchanged (i.e., inversely proportional to N_D).

If the interfacial layer is thin enough, it is reasonable to assume that the interfacial layer is transparent to electrons of sufficient energy to traverse the barrier. The major effect of the interfacial layer upon the V-I characteristics is therefore the change in the barrier height, qV_D.

Equation 17 was stated as

$$j_+ = qN_D\left[\frac{kT}{2\pi m^*}\right]^{1/2} e^{-qV_D/kT} \qquad (17)$$

where

$$V_D = V_{DO} + V$$

In the presence of the interfacial layer, from equation 56 we can show that

$$V_D = V_{DO} + V + \left[V_1^2 + 2V_1\left(\frac{\phi_m - \phi_s}{q}\right)\right]^{1/2} - \left[V_1^2 + 2V_1\left(V + \frac{\phi_m - \phi_s}{q}\right)\right]^{1/2} \qquad (63)$$

where V_{DO} is defined by equation 53. V_{DO} with the interfacial layer is smaller than V_{DO} without the interfacial layer; therefore we can expect a higher leakage current. V_D can be seen to be a slightly weaker function of V in the presence of the interfacial layer.

The Effect of Surface States

The elementary Schottky barrier theory predicts that the barrier height will be directly dependent upon the work functions of the metal used as shown by equation 1. Investigation of this property led to the classic paper by Bardeen (Ref. 12) about the effect of surface states upon barrier height.

The Model of Bardeen was adopted by Cowley (Ref. 7) and Cowley and Sze (Ref. 13) to explain the dependence of barrier height upon surface states. A band diagram of the semiconductor with surface states is shown in figures 5a

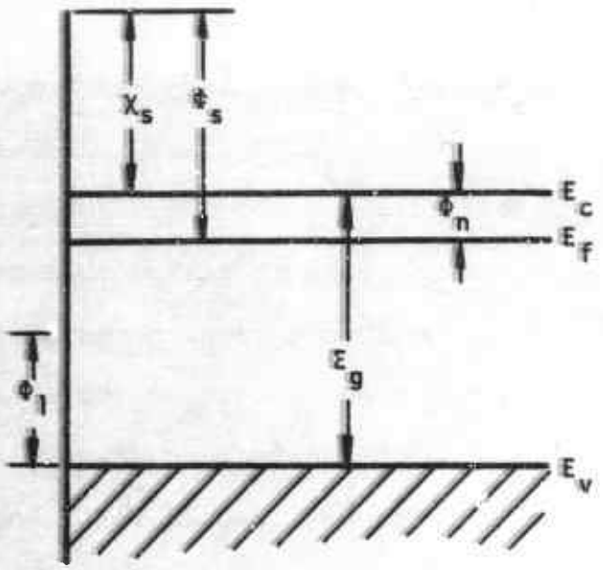

a) Neutral surface, not in thermal equilibrium

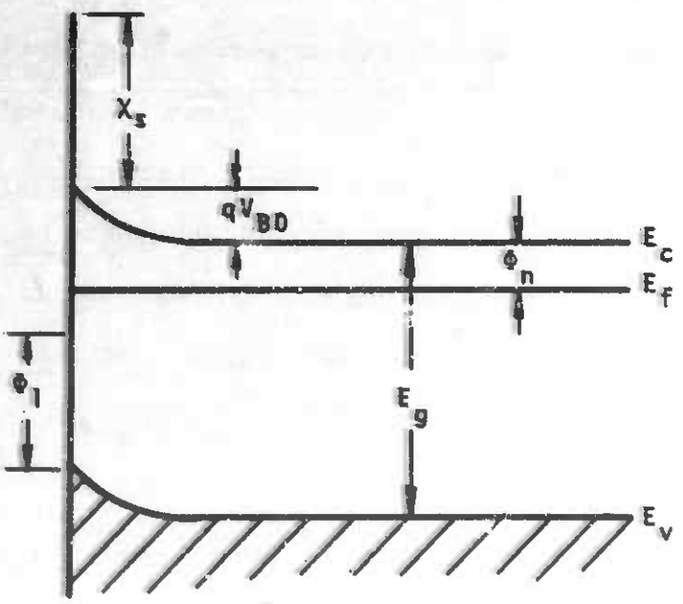

b) Negative surface charge, in thermal equilibrium

Figure 5. Free Semiconductor Surface with Surface States

and 5b. Figure 5a shows the semiconductor not in thermal equilibrium; φ_1 is the energy to which the surface states are filled to obtain charge neutrality on the surface. The surface states that are unfilled and below the Fermi level must be filled for thermal equilibrium. Figure 5b shows the bending of the energy bands when thermal equilibrium is achieved.

A uniform distribution of surface states is assumed above φ_1. The density of states per unit energy per unit area is given by N_s. From equation 10 the charge contained within the space charge distribution is given by

$$Q_{sc} = \sqrt{2q \epsilon_s N_D V_{BO}} \tag{64}$$

where

V_{BO} = potential barrier height necessary for thermal equilibrium

The charge in the surface states, Q_{ss}, can be expressed as

$$Q_{ss} = -2q N_s (E_g - \varphi_n - \varphi_1 - qV_{BO}) \tag{65}$$

The requirement for semiconductor charge neutrality is satisfied by

$$Q_{sc} + Q_{ss} = 0 \tag{66}$$

When this condition is solved for V_{BO} it yields

$$V_{BO} = + \frac{1}{q} (E_g - \varphi_n - \varphi_1) + \frac{\epsilon_s N_D}{4q^3 N_s^2}$$

$$- \left[\frac{1}{q} (E_g - \varphi_n - \varphi_1) \frac{\epsilon_s N_D}{2q^3 N_s^2} + \left(\frac{\epsilon_s N_D}{4q^3 N_s^2} \right)^2 \right]^{1/2} \quad (67)$$

For large N_s, equation 67 reduces to

$$V_{BO} = \frac{1}{q} (E_g - \varphi_n - \varphi_1) \quad (68)$$

The barrier height is fixed and the Fermi level is pinned to φ_1 independent of bulk properties.

Formation of a metal contact is shown in figures 6a and 6b. Before contact there is a potential difference of $1/q\ (\varphi_m - \varphi_s) - V_{BO}$ which must be compensated for by rearranging the charge. A potential drop across the interfacial region also exists. Overall charge neutrality requires

$$Q_m = - (Q_{sc} + Q_{ss}) \quad (69)$$

The potential across the interface can be determined by two methods. From Gauss' law we get

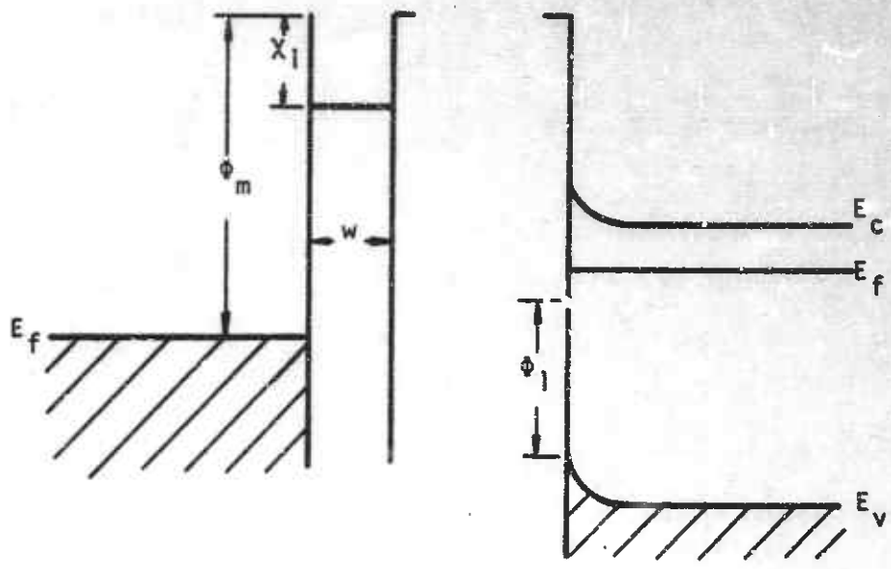

a) Before contact

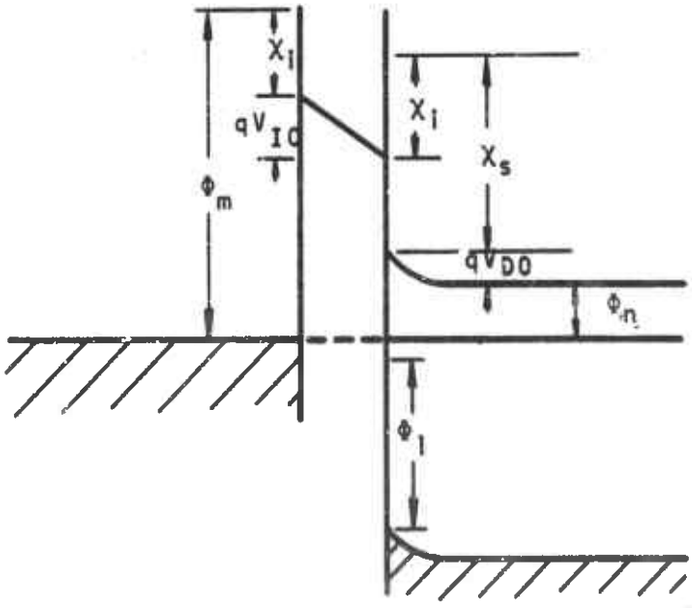

b) After contact

Figure 6. Metal-Insulator-Semiconductor Junction with Surface States

$$E_{io} = -\frac{Q_m}{\epsilon_i}$$

$$V_{io} = -W\frac{Q_m}{\epsilon_i}$$

It follows from equations 64, 65, and 69 that

$$V_{io} = \frac{+W}{\epsilon_i}\left[\left(2q\epsilon_s N_D V_{DO}\right)^{1/2} - 2qN_s\left(E_g - \varphi_n - \varphi_1 - qV_{DO}\right)\right] \tag{70}$$

and from figure 6b

$$V_{io} = \frac{1}{q}\left[\varphi_m - \chi_s - qV_{DO} - \varphi_n\right] \tag{71}$$

Equating equations 70 and 71 and solving for V_{DO}, we get

$$V_{DO} = \frac{\frac{1}{q}(\varphi_m - \chi_s - \varphi_n) + \alpha(E_g - \varphi_n - \varphi_1)}{(1+\alpha q)} + \frac{V_1}{(1+\alpha q)^2}$$

$$\frac{1}{(1+\alpha q)^2}\left[2(1+\alpha q)\left\{\frac{1}{q}(\varphi_m - \chi_s - \varphi_n)\right.\right.$$

$$\left.\left. + \alpha(E_g - \varphi_n - \varphi_1)\right\} V_1 + V_1^2\right]^{1/2} \tag{72}$$

where

$$V_1 = \frac{q\epsilon_s W^2 N_D}{\epsilon_i^2}$$

$$\alpha = \frac{2WqN_s}{\epsilon_i}$$

As the density of surface states becomes large the barrier height given by equation 72 reduces to

$$V_{DO} = \frac{1}{q}(E_g - \varphi_n - \varphi_1) \tag{73}$$

which is the same as the fixed barrier height for a free semiconductor surface with a high density of surface states given by equation 68. When the number of surface states is small, equation 72 reduces to

$$V_{DO} = \frac{1}{q}(\varphi_m - \chi_s - \varphi_n) + V_1 - \sqrt{V_1^2 + \frac{2}{q}(\varphi_m - \chi_s - \varphi_n)V_1} \tag{74}$$

Equation 74 is comparable to equation 53 which gives the barrier height in the presence of an insulating interfacial layer with no surface states.

A different semi-empirical approach to surface states was proposed by Mead (Ref. 14). The following discussion is similar to Mead's. For a more detailed and mathematical analysis of the existence of surface states, see Grimley (Ref. 15) or Shockley (Ref. 16).

Surface states apparently are caused by the termination of the crystal lattice at the surface or by the presence of adsorbed foreign atoms. In the Shockley model, surface states exist only for values of lattice spacing less than a

critical value A (see figure 7). One can argue that for lattice spacing greater than A the surface states are near the band edges. As the lattice spacing gets smaller than A, the surface states move rapidly toward the center of the band gap.

When acceptor-like states are introduced below the Fermi level, they will not be in thermal equilibrium until they become occupied. Some of the electrons in the conduction band will have to fall into these states. This action causes a negative surface charge and a positive space charge to develop. Consequently the energy bands bend upward at the surface in a manner similar to that described earlier for the metal semiconductor junction. Acceptor states above the Fermi level will have nc effect.

If we assume a semiconductor with a small lattice spacing and a high density of surface states, its energy diagram will look like figure 7. As a metal is brought closer to the semiconductor interface, it will cause further upward bending of the energy bands. Any of the filled surface states that are above the Fermi level will give up their electrons to the metal when contact is achieved. Therefore, the effect of the metal upon the barrier height is limited. In materials with larger relative lattice spacing and hence surface states closer to the valence and conduction bands, the barrier height will be more affected

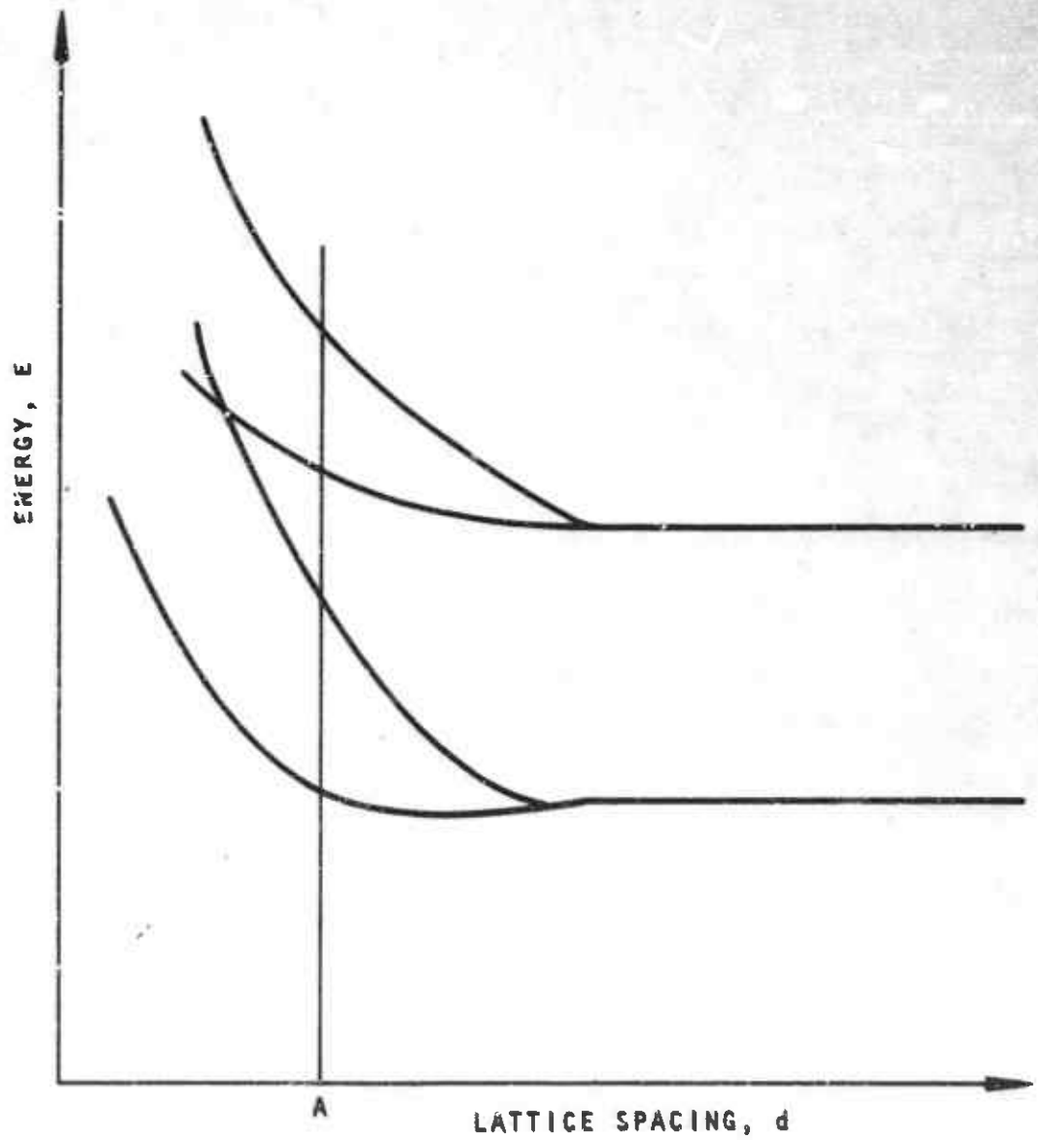

Figure 7. Energy Bands as a Function of Lattice Spacing

by metal work function. Mead and Spitzer (Ref. 17) have found that for most group IV and III-V semiconductors the Fermi level is fixed at a point approximately $E_g/3$ above the valence band edge, where E_g is the width of the band gap.

Mead's model for surface states can be mathematically formulated by assuming that the surface states exist uniformly over a band of width φ_2 at a distance of φ_1 above the valence band edge. Two possible band configurations are illustrated in figures 8 and 9.

In figure 8

$$qV_{DO} < E_g - \varphi_1 - \varphi_2 - \varphi_n \tag{75}$$

The resultant bending of the bands caused by the surface states and the metal is insufficient to raise any of the surface states in φ_2 above the Fermi level. The charge in the surface states is

$$Q_{ss} = -2qN_s\varphi_2 \tag{76}$$

The charge in the depletion region is given by

$$Q_{sc} = \sqrt{2q\epsilon_s N_D V_{DO}} \tag{77}$$

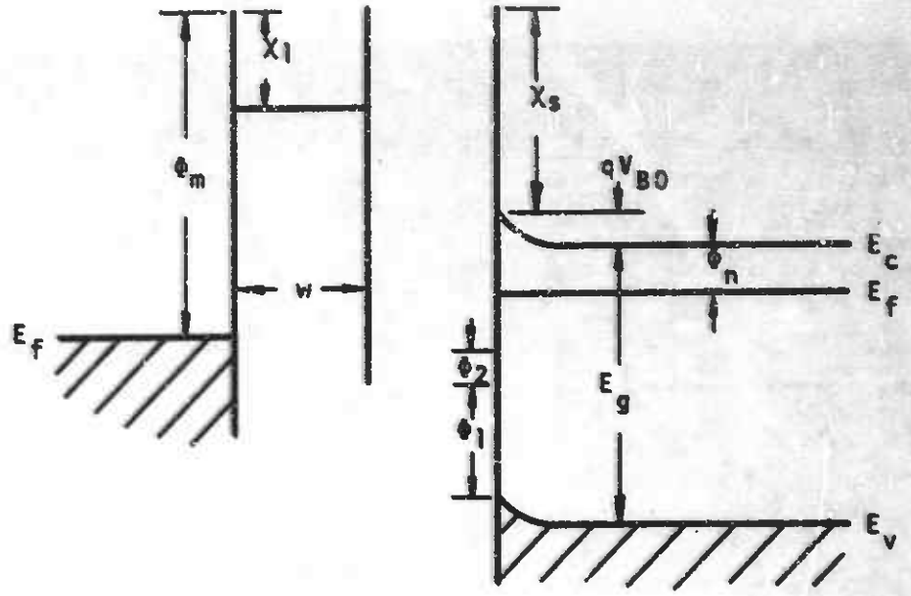

a) Before contact

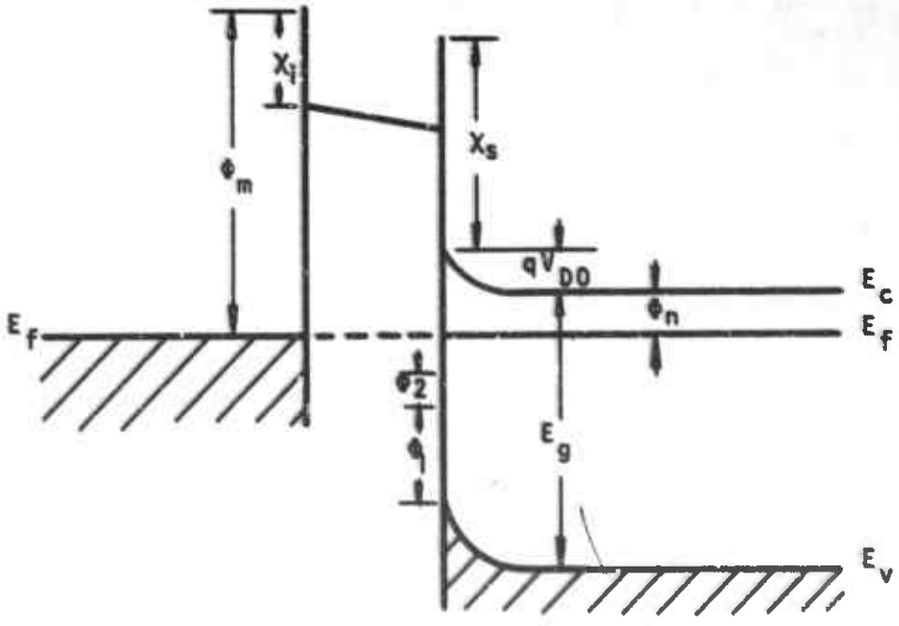

b) After contact

Figure 3. Metal-Insulator-Semiconductor Junction with $qV_{DO} < E_g - \Phi_1 - \Phi_2 - \Phi_n$

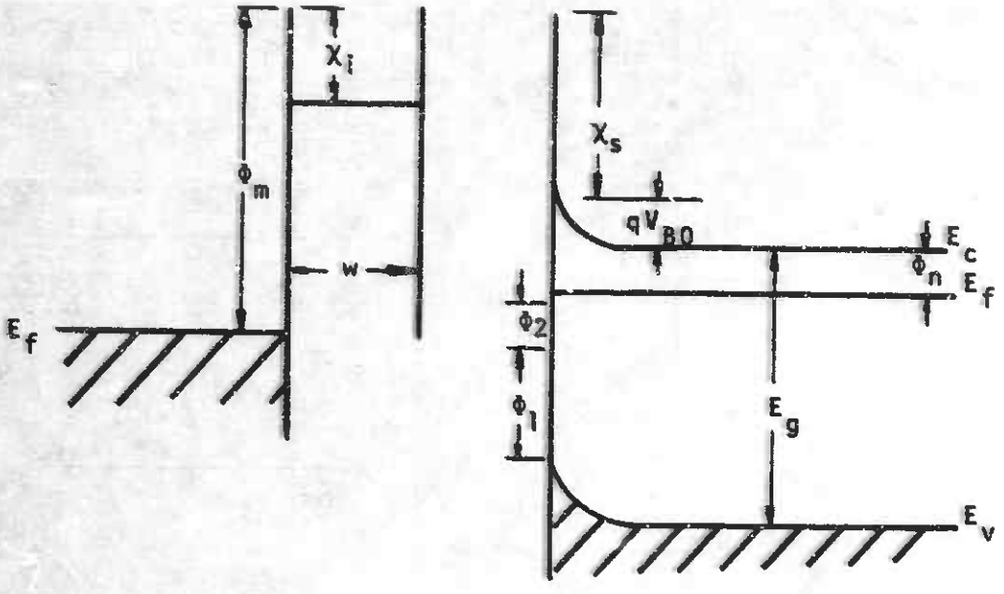

a) Before contact

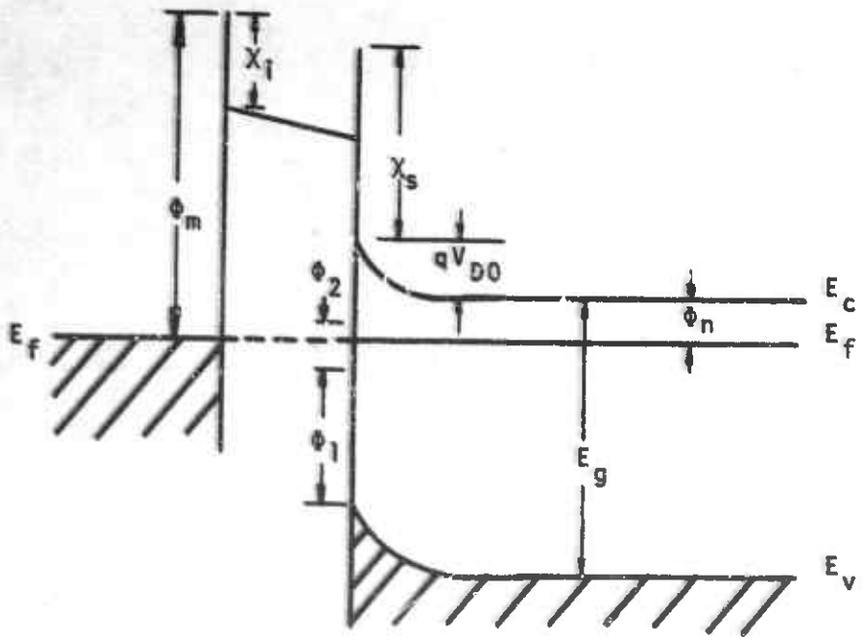

b) After contact

Figure 9. Metal-Insulator-Semiconductor Junction with $qV_{DO} \geq E_g - \phi_1 - \phi_2 - \phi_n$

The charge in the metal is given by equation 69. From consideration of Gauss' law and equality of potentials as explained earlier, we get

$$\frac{1}{q}(\varphi_m - \chi_s - qV_{DO} - \varphi_n) = \sqrt{2V_1V_{DO}} - \alpha\varphi_2 \qquad (78)$$

where V_1 and α are defined following equation 72.

Solving equation 78 for V_{DO} we get:

$$V_{DO} = \frac{1}{q}(\varphi_m - \chi_s - \varphi_n) + \alpha\varphi_2 + V_1 - \sqrt{V_1^2 + 2\left[\frac{1}{q}(\varphi_m - \chi_s - \varphi_n) + \alpha\varphi_2\right]V_1} \qquad (79)$$

In the limit as the number of surface states becomes small, i.e., when α approaches zero, the barrier height, V_{DO}, becomes

$$V_{DO} = \frac{1}{q}(\varphi_m - \chi_s - \varphi_n) + V_1 - \sqrt{V_1^2 + 2\frac{1}{q}(\varphi_m - \chi_s - \varphi_n)V_1} \qquad (80)$$

Equation 80 is comparable to equation 53, the expression for V_{DO} with the presence of an insulating interfacial layer and no surface states. The barrier height increases with surface state density. Therefore, the limit of this case, based upon figure 8, approaches that depicted by figure 9 as the number of surface states becomes large.

In figure 9

$$qV_{DO} \geq E_g - \varphi_n - \varphi_1 - \varphi_2 \tag{81}$$

The distortion of the energy bands will cause a portion of φ_2 to be above the Fermi level; therefore the surface states will not be completely filled. The charge in the surface states is given by

$$Q_{ss} = -2qN_s\left[\varphi_2 - (qV_{DO} + \varphi_n + \varphi_2 + \varphi_1 - E_g)\right]$$

$$= -2qN_s(E_g - \varphi_1 - \varphi_n - qV_{DO}) \tag{82}$$

This is the same as equation 65 in the development of the first model including surface states. The solution for the second case of the model by Mead is the same as the solution of the barrier height for the first model proposed by Bardeen.

Both models show that the barrier height is a function of the density of the surface states. In the limit, as the density of states becomes large, the barrier height becomes fixed and independent of the metal work function.

Effects of Minority Carrier Current

Studies of the minority carriers in Schottky barriers have been performed (Refs. 5 and 18). The conclusions are that in a material where the majority carrier density is much greater than the minority carrier density, the drift and diffusion components of the minority carrier current cancel each other almost exactly. When the majority carrier current density is sufficiently high to cause an electric field to be developed across the bulk material, a more significant minority carrier current component can be expected.

SECTION III

RADIATION EFFECTS ON SCHOTTKY BARRIER DIODES

In this section the effect of transient ionizing radiation on Schottky barrier diodes will be considered. First, it will be instructive to consider the basic interactions of ionizing radiation with matter. Next, the effect of ionizing radiation on a semiconductor will be discussed. Finally, the previous discussions will be applied in the determination of the effect of transient ionizing radiation on Schottky barrier diodes.

Interaction of Ionizing Radiation with Matter

The ionizing radiation to be considered in this paper consists of gamma rays produced by nuclear fission and X rays produced by a high-energy pulsed electron source. In both cases energy exists in the form of photons. These photons interact with matter by four processes: photoelectric, Compton, pair production and photodisintegration.

The photoelectric process tends to dominate for photons of low energies ($\leq$500Kev). The photoelectric effect is the photon electron collision process whereby the incident photon is completely absorbed in the collision. The kinetic energy of the resultant photoelectron is dependent

upon its binding energy to the atom and the energy of the incident photon. The scattering cross section for the photoelectric process decreases with increasing photon energy and increases with increasing z number of the material.

The impinging photon may knock an electron from either an outer or inner atomic shell. If an inner shell electron is knocked out of its position, the atom emits a characteristic X ray in the process of de-excitation.

The Compton effect results more often from a collision of a somewhat higher energy photon and an electron. Compton-type collisions commonly occur for photon energies between 0.2 and 5 Mev. The result of this collision is an energetic electron, a photon of reduced energy, and an atom with an electron missing from the atom. On the average, the electron energy is slightly less than one-half the energy of the incident photon.

Pair production is a reaction that can occur when a high-energy photon interacts with the field of a charged particle or nucleus. The energy of the photon is converted into an electron-positron pair. For this change to be possible, the photon energy must equal at least twice the rest mass energy of an electron or 1.02 Mev. Any excess photon energy is shared as kinetic energy of the electron-positron pair. The pair production process dominates for high Z materials at energies above 5 Mev and at

higher energies for low Z materials. The recombination or annihilation of a zero momentum electron-positron pair results in two 0.51 Mev photons going in opposite directions.

Collisions of high-energy photons (>10 Mev) with a nucleus can cause ejection of protons, neutrons, and α-particles. This process is known as photodisintegration. Photodisintegration is not usually considered as an important process because of the high energies necessary to produce it.

We have now considered the processes by which photons interact with matter. The results of these processes are usually energetic electrons. Therefore, the interactions of energetic electrons will now be discussed.

The electrons lose energy by collision, scattering, and radiation. The creation of Bremsstrahlung is important for high-energy electrons with high Z materials. The collisions are considered to be inelastic collisions with electrons in atoms. Electron scattering is caused by the simple Coulomb interaction between charged particles.

The energy spectrum of the resultant secondary electrons is proportional to $1/E^2$. The higher-energy electrons of the spectrum are capable of producing further ionization. This second generation of electrons will also have a $1/E^2$ energy spectrum The process will continue from generation to generation until none of the remaining electrons

has sufficient energy to cause further ionization. The final distribution of electrons is independent of the primary processes involved.

Effect of Ionizing Radiation upon Semiconductors

Ionizing radiation when discussed in conjunction with semiconductors is of low enough energy that photon interactions by pair production and photodisintegration can usually be neglected. Occasionally an electron of high energy can be created by the photoemission or Compton processes. If this electron suffers a collision with the nucleus, the atom can be knocked out of its proper location in the crystal lattice.

In silicon or germanium semiconductors this damage results in a vacancy and an interstitial atom known as a Frenkel defect. In a III-V compound semiconductor there are eight possible defects caused by displacement or substitution. These defects are: two types of vacancy, two types of substitutional defects, and four possible interstitial configurations. Clearly, separation and cataloging of the effects of these defects for compound semiconductors are more difficult than for silicon or germanium. Fortunately, the number of defects created is typically small when compared with the number of pre-irradiation defects. Therefore, the problem of permanent damage is customarily

neglected in a study of the effect of transient ionizing radiation upon semiconductor devices.

Our primary interest is in the effect of secondary electrons created by the ionization process. Progressing from the individual atom model to the band model of the semiconductor, we find that the secondary electrons exist as free electrons in the conduction band and a corresponding number of free holes exist in the valence band.

Studies of gases and semiconductors in a radiation environment have led to the conclusion that the number of electron-ion pairs created in a material per unit of energy deposited is only a weak function of the target material (Ref. 19). For gases, an electron-ion pair is created for an energy deposited equal to approximately twice the ionization potential. The energy necessary to create an electron-hole pair in a semiconductor is about three to four times the band gap.

Electrons and holes in a semiconductor material move primarily under the influence of electric fields and density gradients. Mobility, μ, describes the excess motion of electrons and holes in an electric field. Mobility in silicon is considered a constant for electric field strength less than 10^4 volts/cm (Ref. 3). The diffusion coefficient, D, describes the motion of holes and electrons by diffusion under a density gradient.

The one-dimensional equations for hole and electron current are given in equations 83 and 84. Since opposite charges attract, we would expect the electron to move toward a positive potential and the hole to move toward a negative potential. These components of current that are influenced by the electric field are commonly called drift current. The diffusion current is a result of the spreading of electrons or holes away from a concentration of carriers.

$$j_n = q \mu_n nE + q D_n \frac{\partial n}{\partial x} \tag{83}$$

$$j_p = q \mu_p pE - q D_p \frac{\partial p}{\partial x} \tag{84}$$

where

j_n = electron current density

j_p = hole current density

q = magnitude of electronic charge

μ_n = electron mobility

μ_p = hole mobility

n = electron concentration

p = hole concentration

E = electric field

D_n = electron diffusion coefficient

D_p = hole diffusion coefficient

Electrons and holes will move as described in equations 83 and 84 until they recombine.

Recombination by direct band-to-band electron-hole annihilation is extremely rare, even in materials such as GaAs where this phenomenon would seem to be highly probable. Usually recombination occurs by a multistep process. Defects in the semiconductor result in recombination centers in the forbidden gap. These defects will capture another one of the free carriers, say a hole; then sometime later the defect will capture an electron and annihilate it. Recombination can be treated mathematically by a technique originally described by Hall (Ref. 20) and Schockley and Read (Ref. 21).

Another process known as trapping will temporarily immobilize electrons or holes. A trap is a defect with a large capture cross section for one of the mobile carriers. The trap will capture the carrier, hold it for a finite time interval, and release it so that it may again contribute to conduction. Traps may immobilize carriers for time periods up to days in duration.

Effect of Ionizing Radiation upon Schottky Barrier Diodes

When a conventional p-n junction is irradiated, an excess of free carriers is produced. The resultant current is dependent upon the radiation pulse intensity and shape, the minority carrier lifetime, minority carrier diffusion length, and applied bias voltage. If the minority carrier lifetimes are short compared to the radiation pulse width, the resultant current pulse will follow the radiation pulse. If the minority carrier lifetimes are long compared to the radiation pulse width, the resultant current pulse will relax to its pre-irradiation value with a characteristic time period.

Under irradiation, electron-hole pairs are generated uniformly throughout the semiconductor. The carriers created in the depletion region are immediately subject to the influence of the relatively strong electric field that exists across this region. The time necessary for the carriers to be swept out of the depletion region is usually much less than the radiation pulse width. To an external circuit, the current created by the motion of the carriers across the depletion region will appear to be instantaneous.

Usually the percentage change in majority carrier density is much less than the percentage change in the minority carrier density. This causes larger carrier

gradients to exist for the minority carriers. Therefore, the minority carriers will dominate the diffusion contribution to the total current.

Most of the radiation-induced diffusion current will be due to excess minority carriers produced within a diffusion length on either side of the junction. Radiation-induced current will flow in a direction so that it will aid leakage current and oppose normal forward current flow. The movement of the excess carriers is determined by the one-dimensional continuity equations (equations 85 and 86).

$$\frac{\partial n}{\partial t} = \frac{n_o - n}{\tau_n} + \frac{1}{q}\frac{\partial}{\partial x} j_n + g \qquad (85)$$

$$\frac{\partial p}{\partial t} = \frac{p_o - p}{\tau_p} - \frac{1}{q}\frac{\partial}{\partial x} j_p + g \qquad (86)$$

where

n_o = thermal equilibrium density of electrons

p_o = thermal equilibrium density of holes

g = generation rate of hole-electron pairs due to an external source

τ_n = minority carrier lifetime for electrons

τ_p = minority carrier lifetime for holes

The continuity equation reflects the time rate of change in carrier density caused by thermal generation and recombination, outward flow of current, and radiation generation.

Substituting equations 83 and 84 into equations 85 and 86 we get

$$\frac{\partial n}{\partial t} = \frac{n_o - n}{\tau_n} + D_n \frac{\partial^2}{\partial x^2} n + \mu_n \frac{\partial}{\partial x}(nE) + g \qquad (87)$$

$$\frac{\partial p}{\partial t} = \frac{p_o - p}{\tau_p} + D_p \frac{\partial^2}{\partial x^2} p - \mu_p \frac{\partial}{\partial x}(pE) + g \qquad (88)$$

Equations 83, 84, 87, and 88 have been solved by Wirth and Rodgers (Ref. 22), van Lint (Ref. 19), et al. Assuming uniform doping concentration, an electric field free region and a rectangular pulse of radiation, the solution is

$$i_{pp}(t) = q\,Ag\left[\left(\ell + L_n \operatorname{erf}\sqrt{t/\tau_n} + L_p \operatorname{erf}\sqrt{t/\tau_p}\right)U(t) - \left(\ell + L_n \operatorname{erf}\sqrt{(t-t_o)/\tau_n} + L_p \operatorname{erf}\sqrt{(t-t_o)/\tau_p}\right)U(t-t_o)\right] \qquad (89)$$

where

$i_{pp}(t)$ = radiation-induced photocurrent

A = junction area

ℓ = depletion layer width

$L_n = \sqrt{D_n \tau_p}$ = diffusion length for electrons

$L_p = \sqrt{D_p \tau_p}$ = diffusion length for holes

$U(t)$ and $U(t-t_o)$ = unit step function turned on at $t = 0$ and $t = t_o$, respectively

Recalling equation 19

$$j = qN_D \left[\frac{kT}{2\pi m^*}\right]^{1/2} e^{-qV_{DO}/kT} \left[e^{-qV/kT} - 1\right] \qquad (19)$$

we can see that the Schottky barrier diode is a majority carrier device. Since the percentage change in majority carrier density is much less than the percentage change in minority carrier density, one would expect a majority carrier device to be less affected by radiation than a minority carrier device. This is the primary reason for making a study of Schottky barrier in a radiation environment.

Figure 10 depicts a Schottky barrier after exposure to ionizing radiation. The excess carriers generated in the depletion region will be swept out by the electric field. These carriers will contribute to the prompt or drift component of the photocurrent. Excess holes created in the bulk region will have a gradient causing a diffusion toward the junction. On the average, holes within a diffusion length of the depletion region will contribute to the diffusion component of the photocurrent. A gradient of electron concentration will not exist on the metal, so no electron diffusion should be expected. From the previous discussion of the p-n junction the resultant photocurrent in the Schottky barrier diode should be

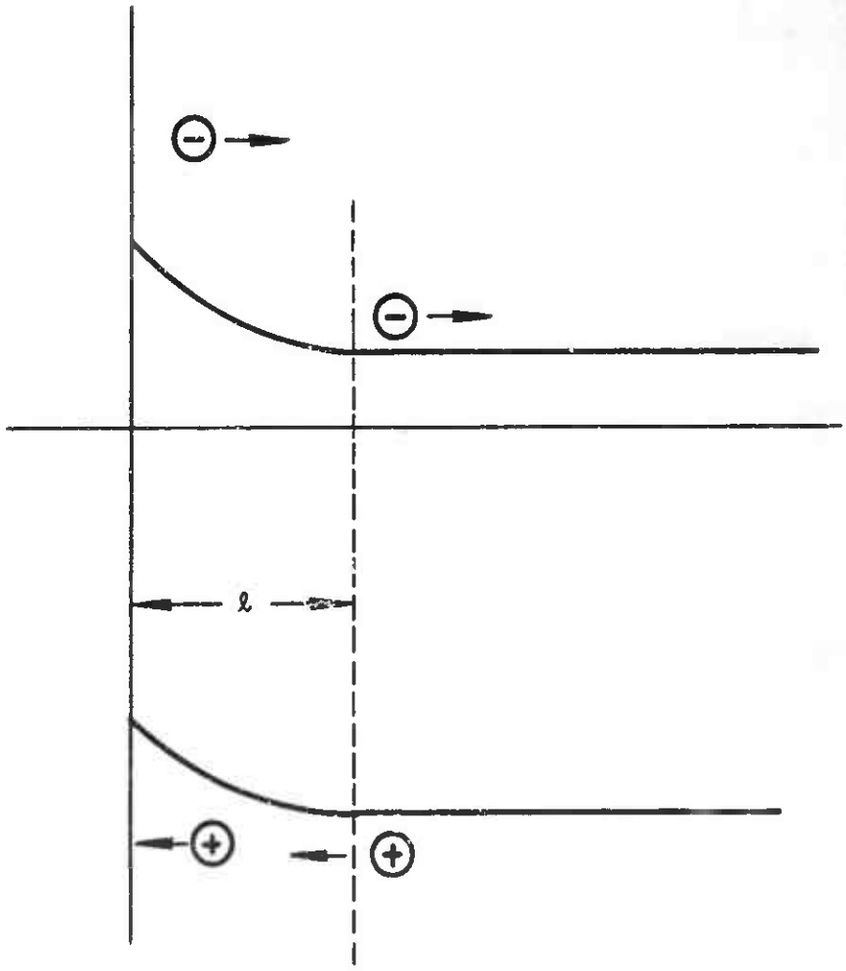

Figure 10. Schottky Barrier During and Immediately After Ionizing Radiation Pulse

$$i_{pp}(t) = q\,Ag\left[\left(\ell + L_p \operatorname{erf}\sqrt{t/\tau_p}\right) U(t)\right.$$

$$\left. - \left(\ell + L_p \operatorname{erf}\sqrt{(t-t_o)/\tau_p}\right) U(t - t_o)\right] \qquad (90)$$

The transient radiation does not affect the parameters of the basic current equation for the Schottky barrier diode. However, a permanent change in the barrier can be caused by a charge trapped in the surface oxide. This mechanism is illustrated in figure 11. During irradiation, electron-hole pairs are created in the oxide. Making the usual assumptions that the holes in the oxide are immobile, the electrons will be attracted to the metal, leaving a net positive charge in the oxide at the semiconductor interface. This charge can cause a distortion in the field configuration in the depletion region. Bell Telephone Laboratories (Ref. 23) noted a small variation in the characteristics of Schottky barrier diodes after heavy irradiation.

A gamma dose of 10^8 rads from a Co^{60} source was found to change the reverse leakage current of an Au-Si diode at 5 volts reverse bias from 5×10^{-8} to 10^{-5} ampere. This dose level is well above those considered in this report; therefore, no further consideration of this effect will be made.

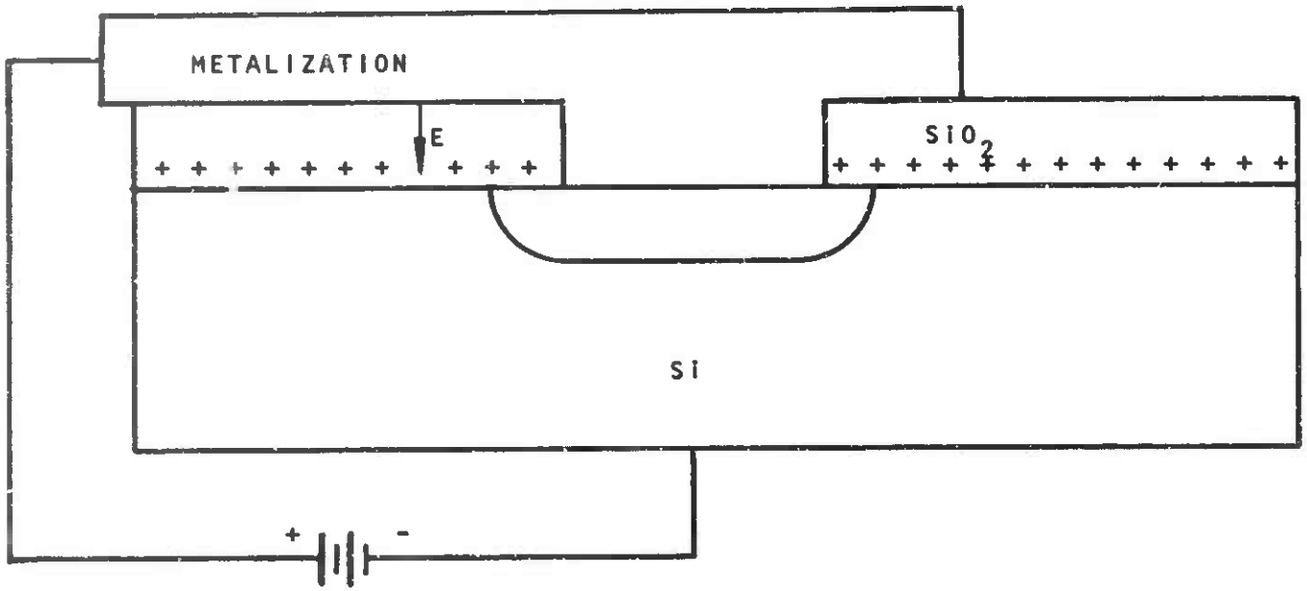

Figure 11. Charge Accumulation in the Oxide Passivation

SECTION IV

EXPERIMENTAL RESULTS

Diode Characteristics

The Schottky barrier diodes used during the experimental portion of this study were produced by Texas Instruments Inc., and have Texas Instruments part numbers TIXV19 and TIV305. The TIV305 is a metal-silicon Schottky barrier diode mounted in a small hermetically sealed glass package. The diode is designed to operate as a UHF mixer. The TIXV19 is a metal-GaAs Schottky barrier diode mounted in a Type E microwave package. The diode is designed to operate as an X-band mixer.

Extensive measurements were performed upon the diodes to determine the diode parameters necessary for prediction of the diode response to an X-ray pulse. The junction area was determined by breaking the top off the diode packages and using a microscope to measure the diode geometry. The TIXV19 had a circular junction with a diameter of 10.5×10^{-6} meter and a circular bonding pad of 27.4×10^{-6} meter in diameter as shown in figure 12a. The TIV305 has a circular junction that is 30.55×10^{-6} meter in diameter and a circular bonding pad that is 126.3×10^{-6} meter in diameter, as shown in figure 12b.

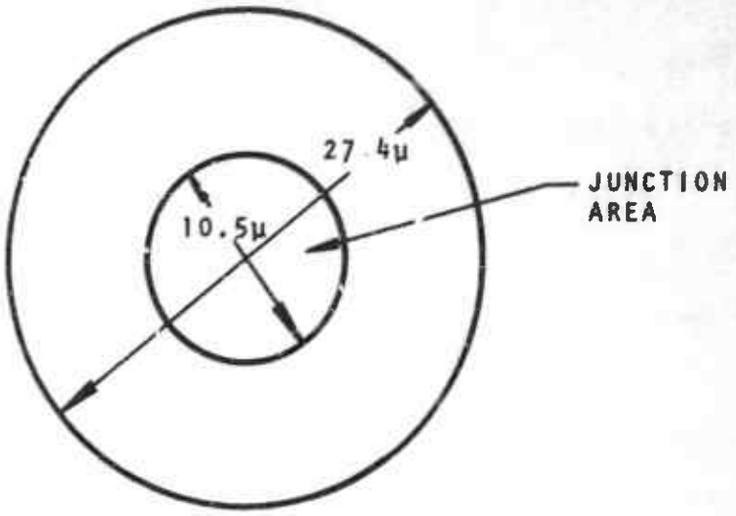

a) TIXV19 Geometry

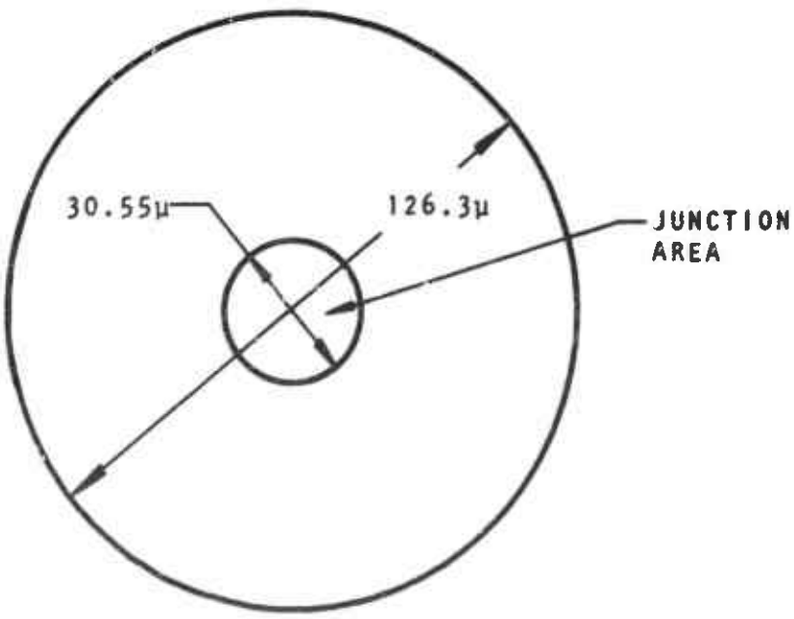

b) TIV305 Geometry

Figure 12. Schottky Barrier Diode Geometries

The capacitance-voltage characteristics were measured for each type of diode using a Boonton Model 75A-S8 capacitance bridge. A capacitance-voltage plot was made for each diode on a semi-automatic capacitance measuring system borrowed from Sandia Corporation. Typical curves are shown in figure 13.

The package capacitance was subtracted from the capacitance-voltage curves and the resultant data were used to create plots of $1/C^2$ vs V. These plots are shown for the TIXV19 and TIV305 in figures 14 and 15, respectively.

Before attempting determination of the barrier height and doping concentration from figures 14 and 15, the construction of the diodes should be taken into consideration. Equation 9 shows that the maximum electric field is proportional to the majority carrier doping concentration N_D. Therefore, in order to achieve a high reverse breakdown voltage, a diode should be made from a material of low dopant concentration. An increase of dopant concentration will decrease the series resistance of the diode; this is also desirable.

These conflicting requirements on N_D are resolved in the case of the TIXV19 and TIV305 by growing a thin lightly doped epitaxial layer on top of a heavily doped substrate as shown in figure 16.

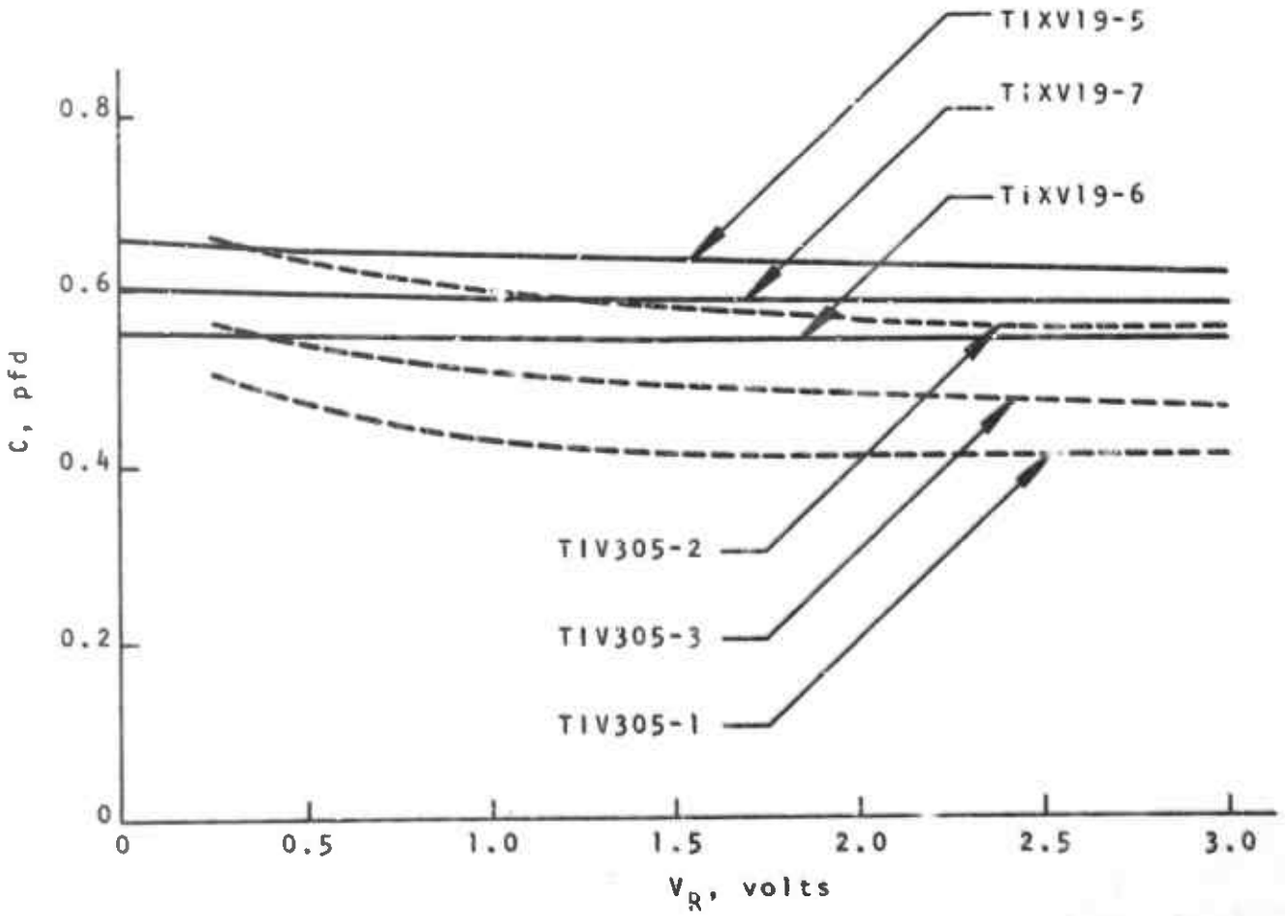

Figure 13. Capacitance versus Voltage for TIXV19 and TIV305 Diodes

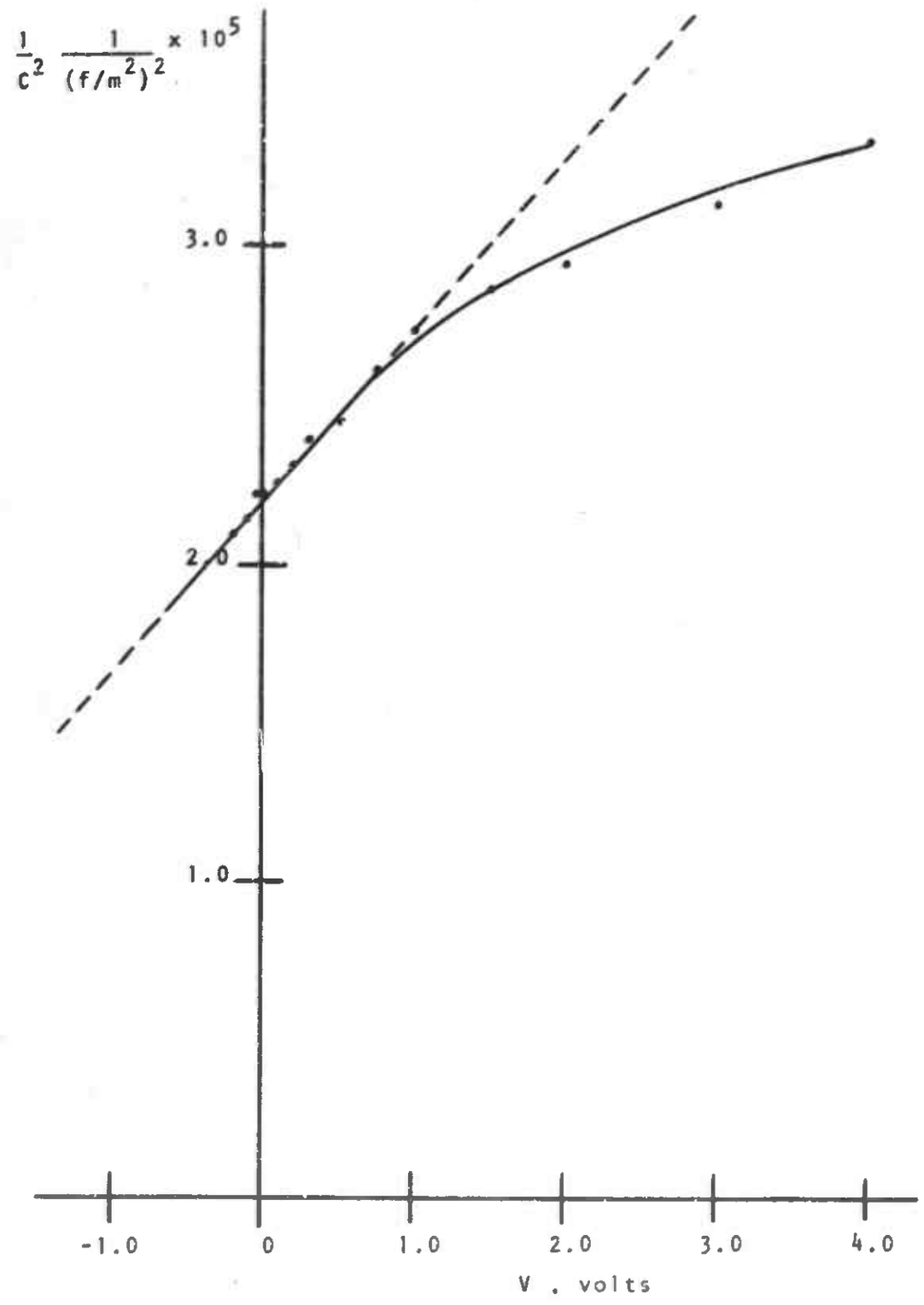

Figure 14. $1/C^2$ versus V for a TIXV19 Schottky Barrier Diode

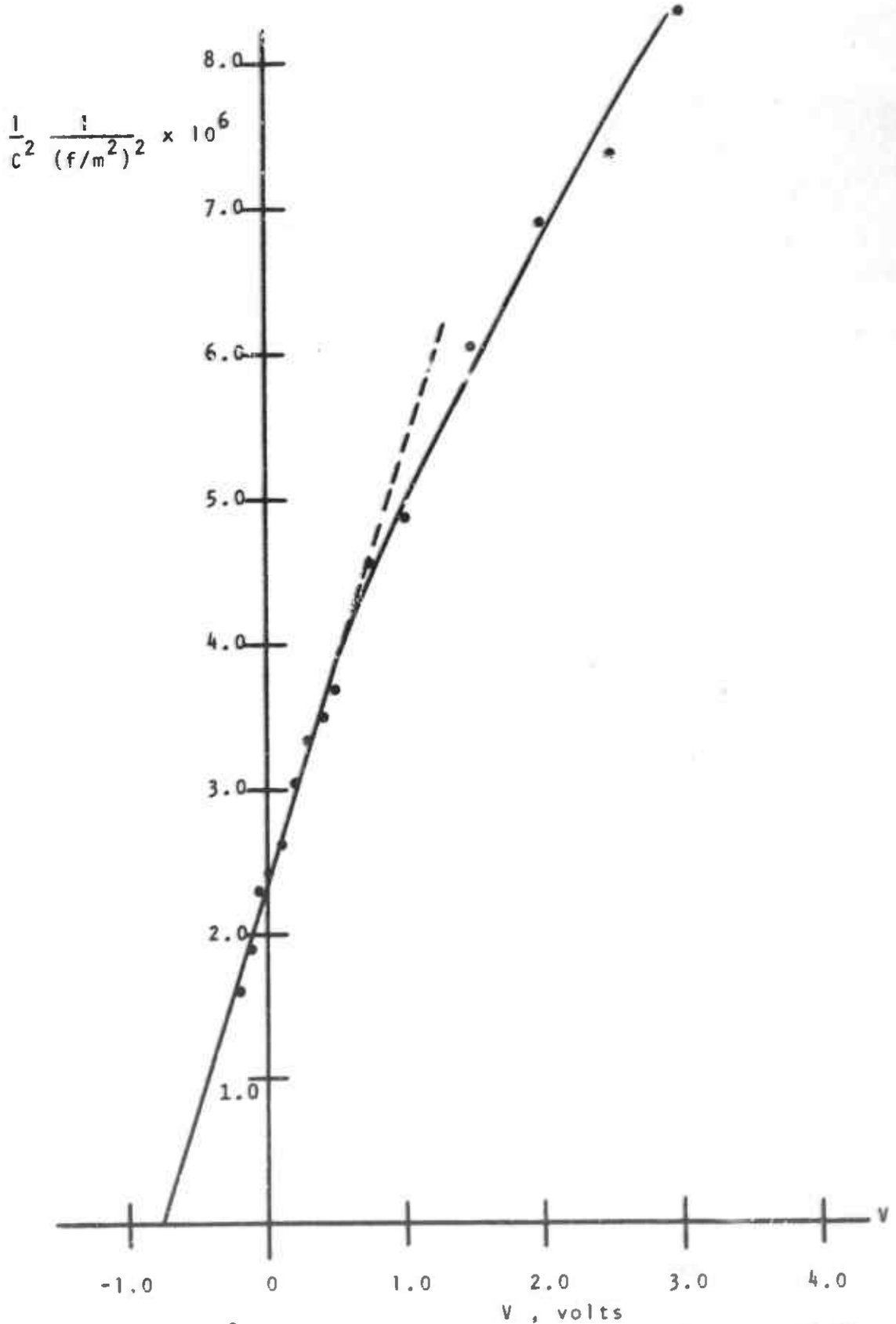

Figure 15. $1/C^2$ versus V for a TIV305 Schottky Barrier Diode

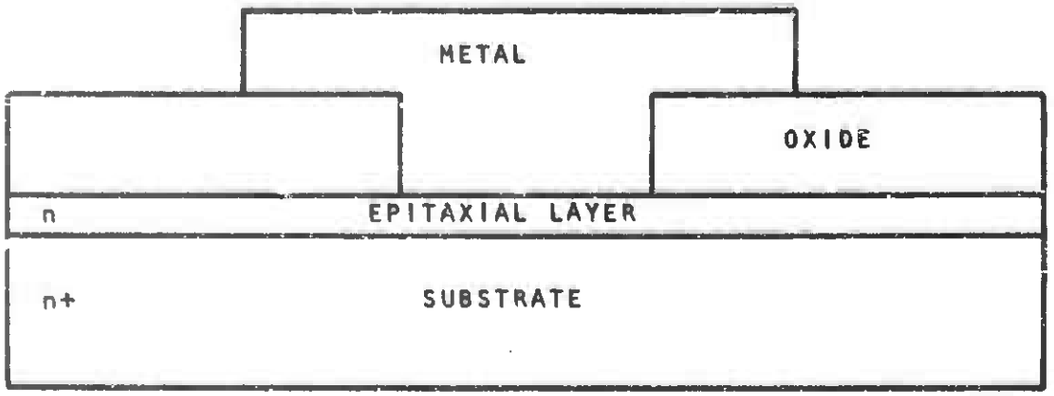

Figure 16. Construction Profile of a Typical Schottky Barrier Diode

Impurities diffuse from the heavily doped substrate into the lightly doped epitaxial layer during the epitaxial growth process, creating a finite impurity gradient. This impurity gradient is the reason that the $1/C^2$ vs V plots are not linear.

Equations 12 and 13 in conjunction with figures 14 and 15 can be used to determine the barrier height, V_{DO}, and the dopant concentration, N_D. Restating equation 12,

$$\frac{1}{C^2} = \frac{2}{\epsilon_s N_D q} (V_{DO} + V) \tag{12}$$

we recall that $V_{DO} = -V$ when $1/C^2 = 0$.

An extrapolation of the curve in figure 14 gives a V axis intercept of -4.06 volt, which does not compare favorably with barrier heights of 0.94, 0.95, and 0.97 volt given in references 24, 17, and 25, respectively. similar extrapolation in figure 15 results in a barrier height of 0.77 volt which compares favorably with the values of 0.78, 0.79, and 0.80 volt given by references 17, 26, and 27, respectively.

$$\frac{d(1/C^2)}{dV} = \frac{2}{\epsilon_s N_D q} \tag{13}$$

From equation 13, repeated above, we recall that the majority carrier dopant concentration, N_D, is inversely proportional to the slope of the $1/C^2$ vs. voltage curve. The slope of the curves in figures 14 and 15 are 5.4×10^4 and 3.04×10^6 $(meters^4)/(volt\text{-}farad^2)$, respectively.

The parameters tabulated below were used in the calculations to follow:

	Silicon	GaAs
ε_s	$11.7\ \varepsilon_o$	$11.6\ \varepsilon_o$
ρ	$2330\ kg/m^3$	$5300\ kg/m^3$
E_i	3.36 ev	4.38 ev
τ_p	10^{-7} sec	2.2×10^{-8} sec
D_p	$6.5\ cm^2/V\text{-}sec$	--
L_p	8×10^{-6} m	3.5×10^{-6} m
A	$6.45 \times 10^{-10}\ m^2$	$8.65 \times 10^{-11}\ m^2$
V_{DO}	0.78 V	0.94 V
N_D	$3 \times 10^{22}\ m^{-3}$	$10^{22}\ m^{-3}$

The symbol A is the area of the silicon TIV305 Schottky barrier diode and the gallium arsenide TIXV19 Schottky barrier diode. Typical values of barrier height, V_{DO}, were taken as discussed in References 17, 24, 25, 26, and 27. The values of N_D are considered typical of the devices studied.

Calculations from the experimental data and equation 13 show an N_D of 2.27×10^{24} atoms/meter^3 for the TIXV19 GaAs diode. This value is about two orders of magnitude too large. Similar

calculations give an N_D of 3.98×10^{22} atoms/meter^3 for the TIV305 silicon diode, which is the proper order of magnitude.

The discrepancies between the expected and measured results for the TIXV19 diode are a result of inaccuracies inherent in the measurement of their capacitances. The Type E microwave diode package has a nominal capacitance of 5.5×10^{-13} farad. The calculated capacitance of an idealized GaAs Schottky barrier diode with a junction area of 8.65×10^{-11} meter^2 is 4.2×10^{-14} farad. The capacitance of the Schottky barrier diode and its variation with voltage is two orders of magnitude smaller than the capacitance of the package alone. Therefore, it is impossible to resolve the true capacitance variation of the GaAs diode capacitance with voltage because of the much greater package capacitance.

The calculated capacitance of a silicon Schottky barrier diode with a junction area of 6.45×10^{-10} meter^2 is 3.68×10^{-13} farad at zero applied bias voltage. The package in which the diode is mounted has a capacitance of approximately 3.5×10^{-13} farad. Although the ratio of diode capacitance to package capacitance is far from ideal, it is reasonable that better correlation was obtained between measured and calculated values for the TIV305.

Typical current voltage curves are shown in figures 17 and 18 for the TIXV19 and TIV305, respectively. The deviation

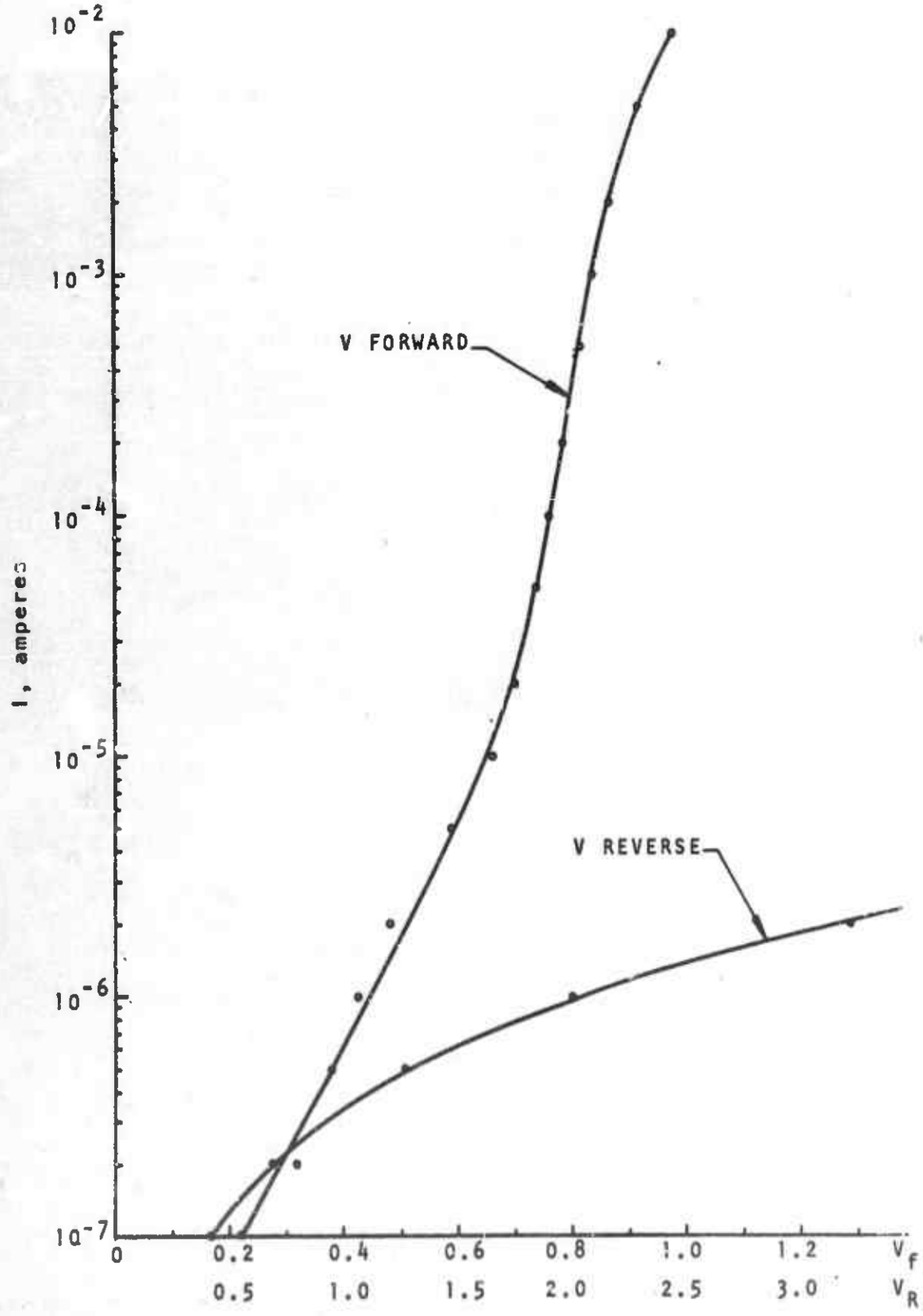

Figure 17. Current versus Voltage for a TIXV19 Schottky Barrier Diode

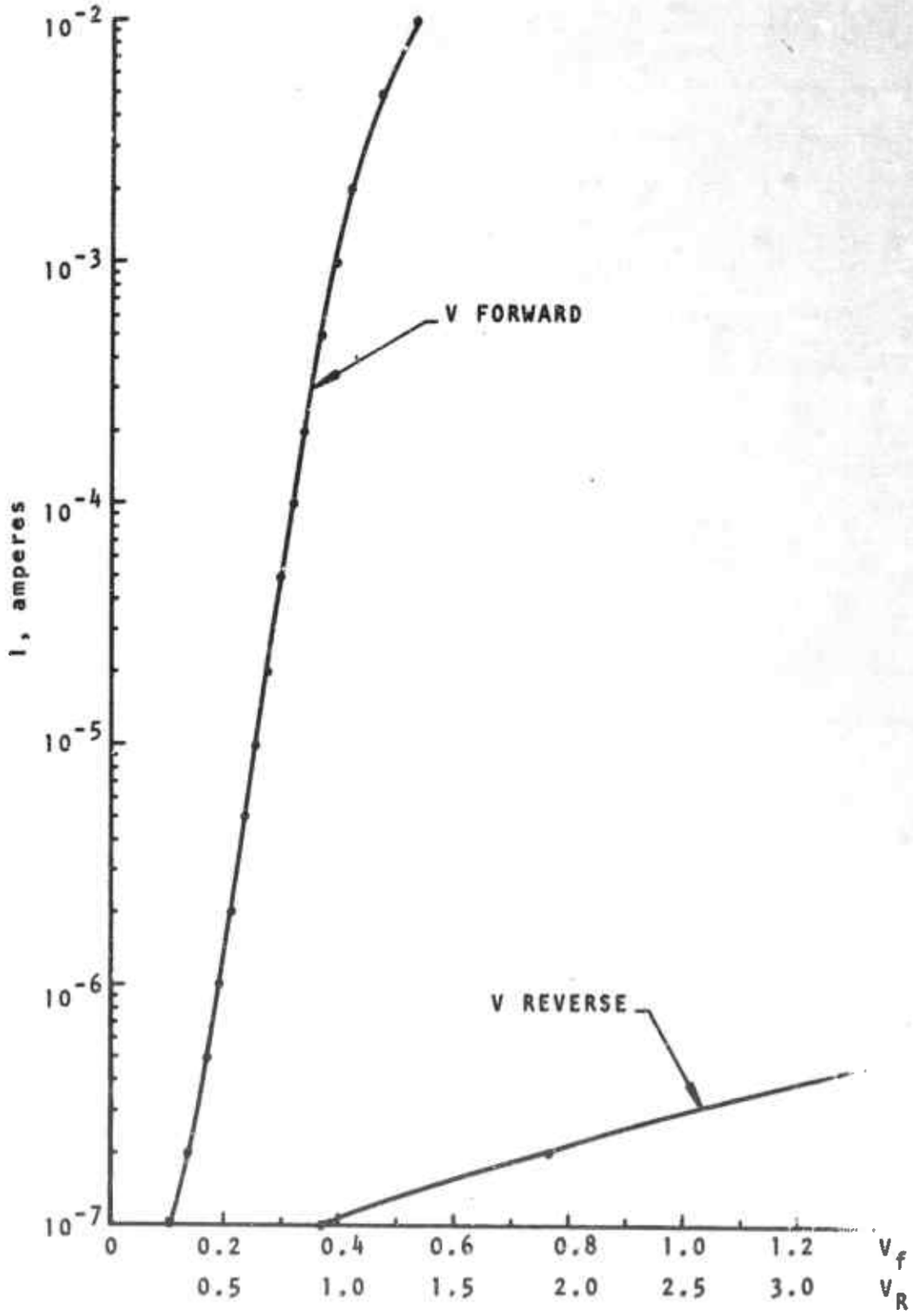

Figure 18. Current versus Voltage for a TIV305 Shottky Barrier Diode

from a straight line at high currents is caused by the series resistance of the diode. The deviation at low currents is not reproducible and is apparently caused by surface conditions.

The peak photocurrent can be predicted by use of equation 90

$$i_{pp} = q\,Ag\left\{\left(\ell + L_p \operatorname{erf}\sqrt{t/\tau_p}\right) U(t) - \left(\ell + L_p \operatorname{erf}\sqrt{\frac{t - t_o}{\tau_p}}\right) U(t - t_o)\right\} \quad (90)$$

The generation rate, g, is calculated from equation 91

$$g = 6.25 \times 10^{16} \frac{R\rho}{E_i} \quad (91)$$

where

R = dose rate in rads/sec

ρ = density of material irradiated in kg/m^3

E_i = energy necessary to produce one electron-hole pair in electron volts (this is assumed to be about three times the forbidden band gap energy.)

The dose rate at which the silicon and gallium arsenide Schottky barrier diodes were exposed was approximately 6.7×10^8 rad/sec or 20 rads in 30 nanoseconds. The calculated generation rates for GaAs and silicon are 4.2×10^{28}

and 2.9×10^{28} electron hole pairs/second-meter^3, respectively. These calculations were based on equation 91. Note that equation 90 consists of two types of terms. The terms which depend upon ℓ arise from the photocurrent generated within the depletion region and is called prompt photocurrent. The terms which depend upon L_p arise from the diffusion of holes from the bulk region of the semiconductor to the metal/semiconductor junction. According to equation 90, the photocurrent current will be a maximum at $t = t_o^-$, the end of an assumed square wave radiation pulse, and is the sum of the prompt and diffusion components of photocurrent at that time. For our calculations t_o = 30 nanoseconds.

From equation 4, the depletion width of the TIXV19 GaAs diode is 3.47×10^{-7} meters at zero bias. This calculation is based on a doping concentration $N_D = 10^{22}$ atoms/meter^3. Using equation 90, and the tabulated parameters for the TIXV19 diode, the prompt, diffusion, and maximum photocurrents are 0.2×10^{-6} ampere, 1.8×10^{-6} ampere, and 2.0×10^{-6} ampere, respectively. The value of τ_p as tabulated was obtained from reference 28.

A similar calculation for the silicon TIV305 diode yields prompt, diffusion and total photocurrents of 0.5×10^{-6}, 13.5×10^{-6} and 14.0×10^{-6} amperes, respectively. The value of N_D used in determining the parameter ℓ_o was 3×10^{22} atoms/meter^3, a value typical of this device.

It is interesting to compare theoretical maximum photocurrents for GaAs diodes and silicon diodes of the same junction area using doping concentrations typical of the TIXV19 and TIV305. It follows from equations 4, 90, and 91 and the stated parameters of these devices that the photocurrent of the GaAs diode would be 1.07 times the silicon diode photocurrent, for a given dose of flash X rays of 30 nanoseconds duration. If the dopant concentrations were the same, this factor would become 1.16. We conclude that silicon and gallium arsenide Schottky barrier diodes should produce photocurrents per unit junction area which are about the same value for a given dose and dose rate and for the parameters typical of the TIXV19 and TIV305 diodes.

Results of Tests Using Flash X-Ray Machine

The experiments covered in this section were performed at Kirtland Air Force Base, Air Force Weapons Laboratory, using a Field Emission Corporation Febetron Model 705 two-million-volt pulsed radiation source. A detailed description of the source, test facilities, and equipment is contained in Appendix II.

The TIXV19 GaAs Schottky barrier diode was tested as a conventional diode, as a detector diode, and as a mixer diode. The TIV305 silicon Schottky barrier diode was tested as a conventional diode. The voltage-current characteristics were monitored periodically during testing. The noise figure of the diode was monitored while it was being tested as a mixer. Dosimetry was obtained from the thermoluminescence of lithium-fluoride-impregnated teflon disks.

Testing of the diodes as conventional diodes was performed, using the circuit shown in figure 19. In a typical test configuration all of the circuit except the diode under test was shielded from the X-ray beam by at least 4 inches of lead. Spurious effects were minimized by keeping all wirelengths short and decoupling the power supply.

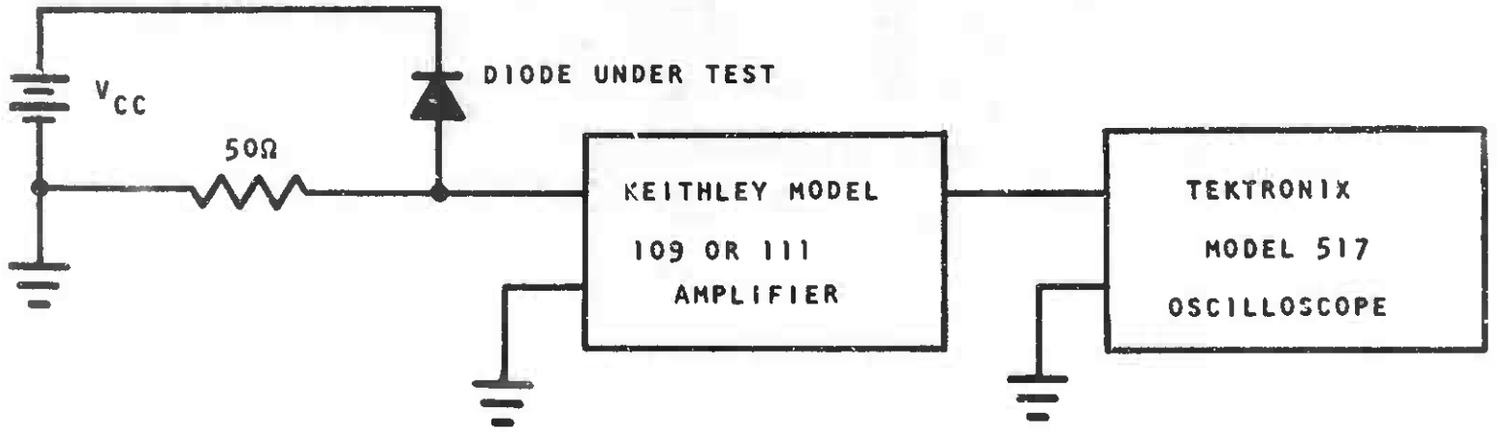

Figure 19. Conventional Diode Test Circuit

The TIXV19 GaAs Schottky barrier diodes were connected as shown in figure 19 by means of a waveguide diode holder and were exposed to an X-ray pulse of 3×10^{-8} second duration. Total dose of a single pulse was approximately 20 rads. The resultant peak photocurrent was 1.99×10^{-3} and 3×10^{-4} ampere for reverse bias voltages of 1.0 and zero volts, respectively. The peak photocurrent was two to three orders of magnitude larger than the 2.13×10^{-6} and 2.09×10^{-6} ampere predicted by equation 90.

The waveguide diode holder was removed from the circuit and the diode was connected into the test circuit by soldering. The resultant peak photocurrent was changed to 1.0×10^{-3} and 8.7×10^{-4} ampere under the same bias conditions. Typical waveforms are shown in figures 20 and 21.

The TIV305 silicon Schottky barrier diodes were exposed to similar X-ray pulses. The resultant peak photocurrent was 2.30×10^{-3} and 2.28×10^{-3} ampere for a reverse bias of 1.0 and 0.0 volt, respectively, as shown in figure 22. These values are also considerably larger than the expected values of 1.44×10^{-5} and 1.41×10^{-5} ampere.

The difference between the expected peak photocurrent and the experimentally observed peak photocurrent was too large to be explained by normal experimental or equipment-induced errors. Therefore an extensive testing program was undertaken to isolate the source of the excess photocurrent.

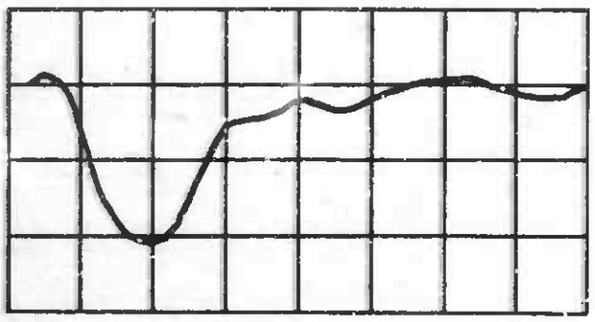

a) TIXV19-1
V_R = 1.0
Horizontal 20ns/cm
Vertical 20mv/cm
Dose rate = 6.7×10^8 rads/sec

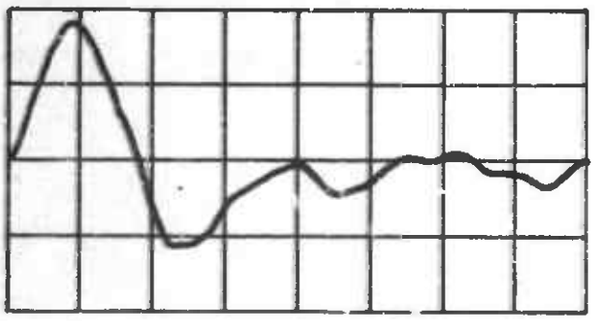

b) TIXV19-1
V_R = 0.0
Horizontal 20ns/cm
Vertical 10mv/cm
Dose rate = 6.7×10^8 rads/sec

Figure 20. Response of GaAs Schottky Barrier Diode in Waveguide to X-ray Pulse

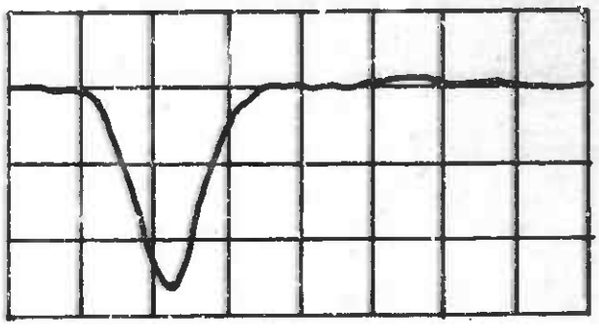

a) TIXV19-3

V_R = 1.0

Horizontal 20ns/cm

Vertical 20mv/cm

Dose rate = 6.7 x 10^8 rads/sec

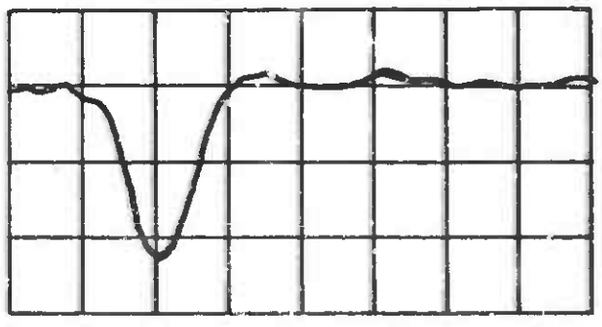

b) TIXV19-3

V_R = 0.0

Horizontal 20ns/cm

Vertical 20mv/cm

Dose rate = 6.7 x 10^8 rads/sec

Figure 21. Response of GaAs Schottky Barrier Diode to X-ray Pulse

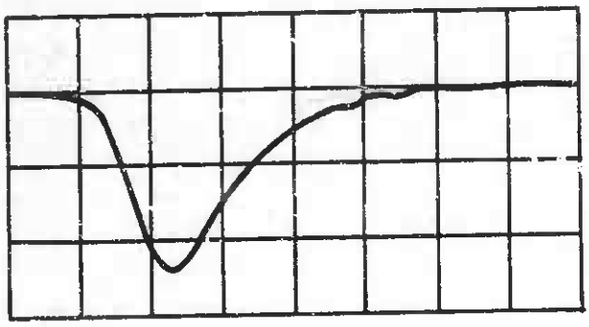

a) TIV305-1
V_R = 1.0
Horizontal 20ns/cm
Vertical 50mv/cm
Dose rate = 6.7×10^8 rads/sec

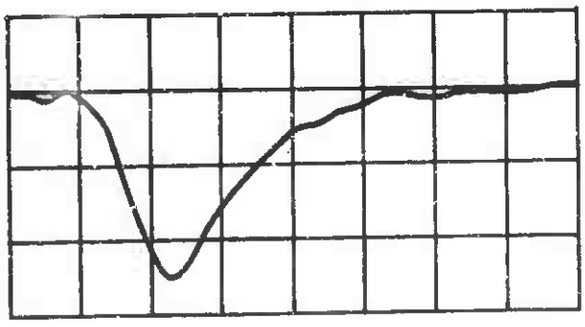

b) TIV305-1
V_R = 0.0
Horizontal 20ns/cm
Vertical 50mv/cm
Dose rate = 6.7×10^8 rads/sec

Figure 22. Response of Silicon Schottky Barrier Diode to X-ray Pulse

One of each of the two types of diode packages that exhibited more than 10^{10} ohms between its terminals was obtained. The packages were obtained by subjecting a good diode to a current surge from a discharging capacitor. The resultant package, when irradiated, was expected to behave in the same manner as before except that any contribution from the diode junction had been eliminated. The peak photocurrents obtained experimentally from the packages were very nearly identical to the results obtained from good diodes.

Insertion of 4 inches of lead between the package under test and the X-ray source eliminates the photocurrent. This shows that the photocurrent is a direct or indirect result of the radiation.

Further experimental testing showed that a similar photocurrent could be obtained by extending a wire about 0.75 inch long into the X-ray beam.

The photocurrent was of the polarity that required electron flow from the test wire through the viewing resistor to ground. Several possible sources of the spurious signal exist. Possible sources include collection of electrons knocked out of adjacent materials, the large electromagnetic pulse that exists during the creation of the X-ray pulse, ground currents, transients induced on the power line, etc.

Because of the spurious response that exists in any experimental test configuration, the only way to experimentally prove the validity of equation 90 is to test diodes whose true response is greater than the spurious response. In the case of Schottky barriers, the peak photocurrent can be increased by increasing the junction area or by decreasing N_D. Neither of these solutions can be tried at this time because The University of New Mexico does not currently have facilities capable of producing Schottky barrier diodes and because the cost involved in having an outside source produce Schottky barrier diodes to our specifications is prohibitive.

The TIXV19 GaAs Schottky barrier diode was also tested as a detector. The test circuit is shown in figure 23. The oscillator output was set at 9.375 GHz and 1.0×10^{-3} watt. The photocurrent was determined as a function of applied bias voltage and current. The sliding short was adjusted to obtain a maximum DC voltage out of the detector for each bias condition. The AC transient caused by the X-ray pulse was then observed.

The peak photocurrent as a function of applied bias was approximately the same as before, without the microwave signal. The peak photocurrent as a function of DC bias current is shown in figure 24.

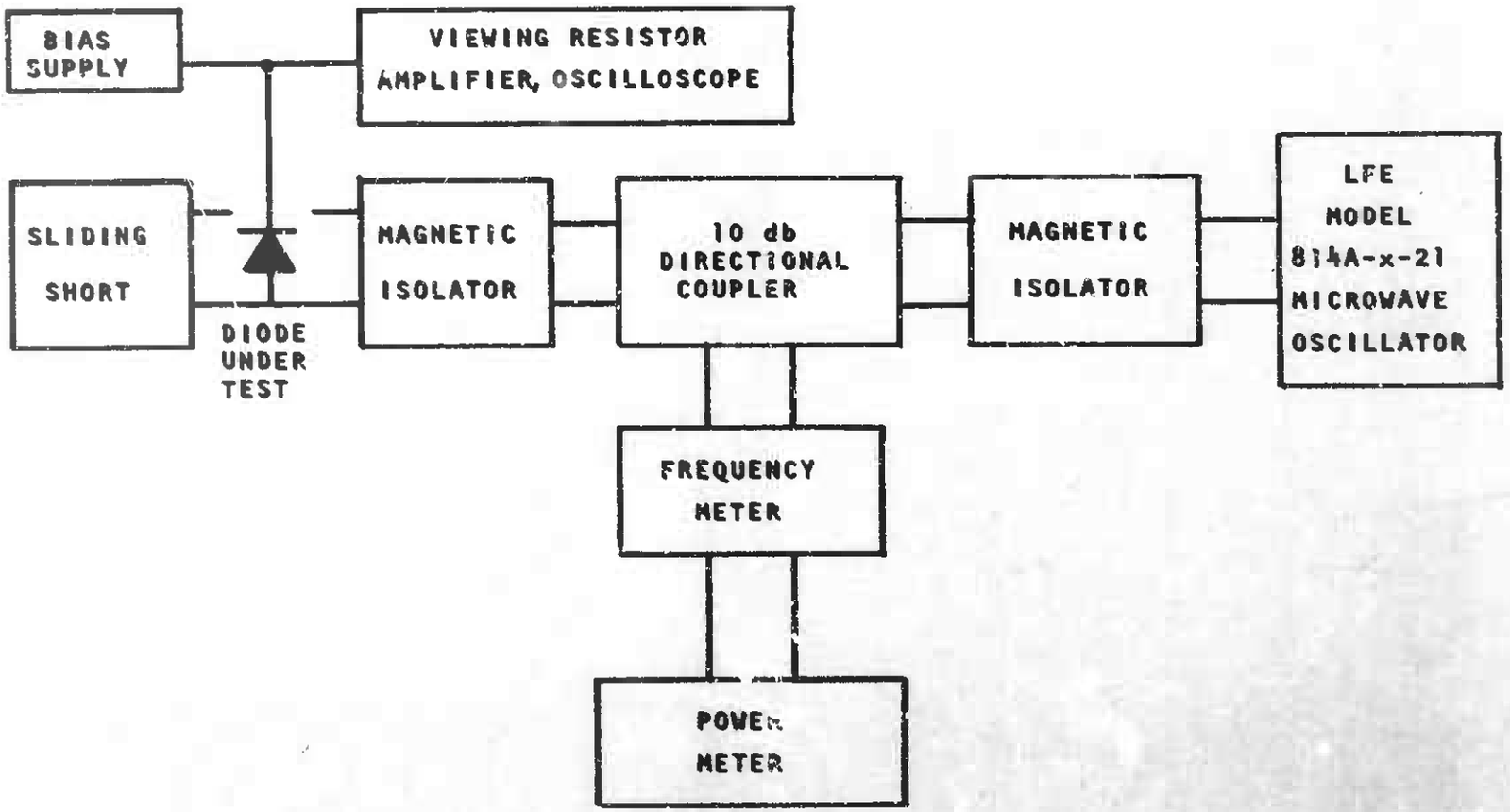

Figure 23. Circuit for Testing GaAs Schottky Barrier Diode as an X-band Detector Diode

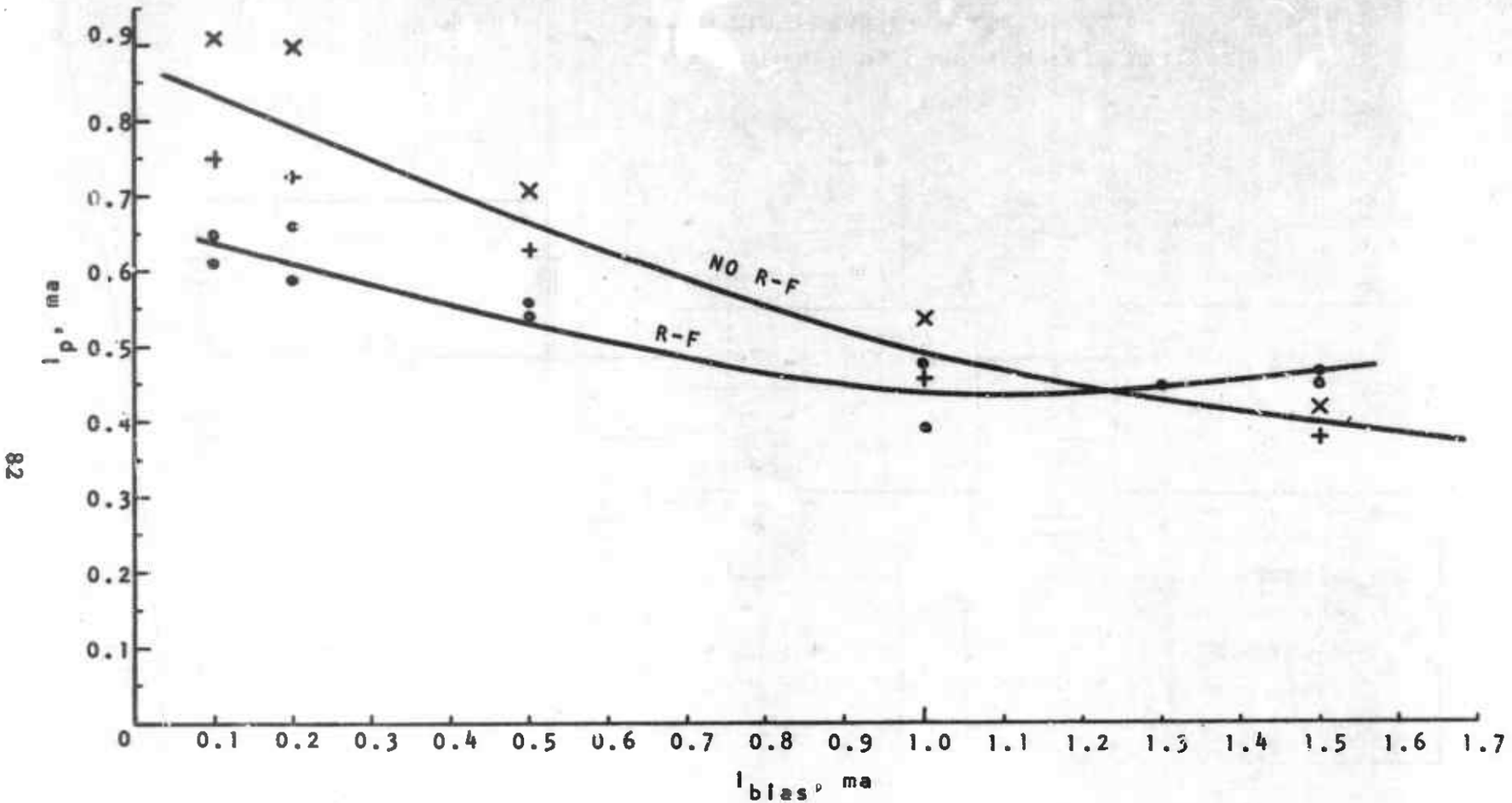

Figure 24. Peak Photocurrent versus Bias Current for TIXV19 Detector Diode

A minimum peak photocurrent occurs between 9×10^{-4} and 1.3×10^{-3} ampere forward bias. The minimum occurs only when the microwave signal is present.

The TIXV19 GaAs Schottky barrier diode was also tested as a mixer diode. The test circuit is shown in figure 25. A magic tee was used to mix the signals from the two signal generators. A microwave signal entering the E arm of the magic tee is split in two parts with half of the signal going into each of the straight-through arms and no signal coupled into the H arm. Conversely, a signal entering the H arm is split with no coupling to the E arms. Magnetic isolators were used in each arm to prevent propagation of reflections back into the magic tee. The local oscillator was set at a frequency of 9.375 GHz with a power at the diode of 1.0×10^{-3} watt. The oscillator in the antenna leg was set at a frequency of 9.405 GHz or 9.345 GHz. The power level was adjusted to achieve a predetermined signal out of the mixer diode.

The mixer diode was connected to a DC bias source and an I-F amplifier with an input impedance at 30 MHz of 50 ohms. The amplifier has a gain of 48 db, a center frequency of 30 MHz, and a bandwidth of 8 MHz.

For noise figure measurement the antenna leg oscillator was replaced by a Hewlett-Packard Model X-347A noise source. The output of the amplifier was then fed into a Hewlett-Packard Model 342A noise figure meter. The noise figure

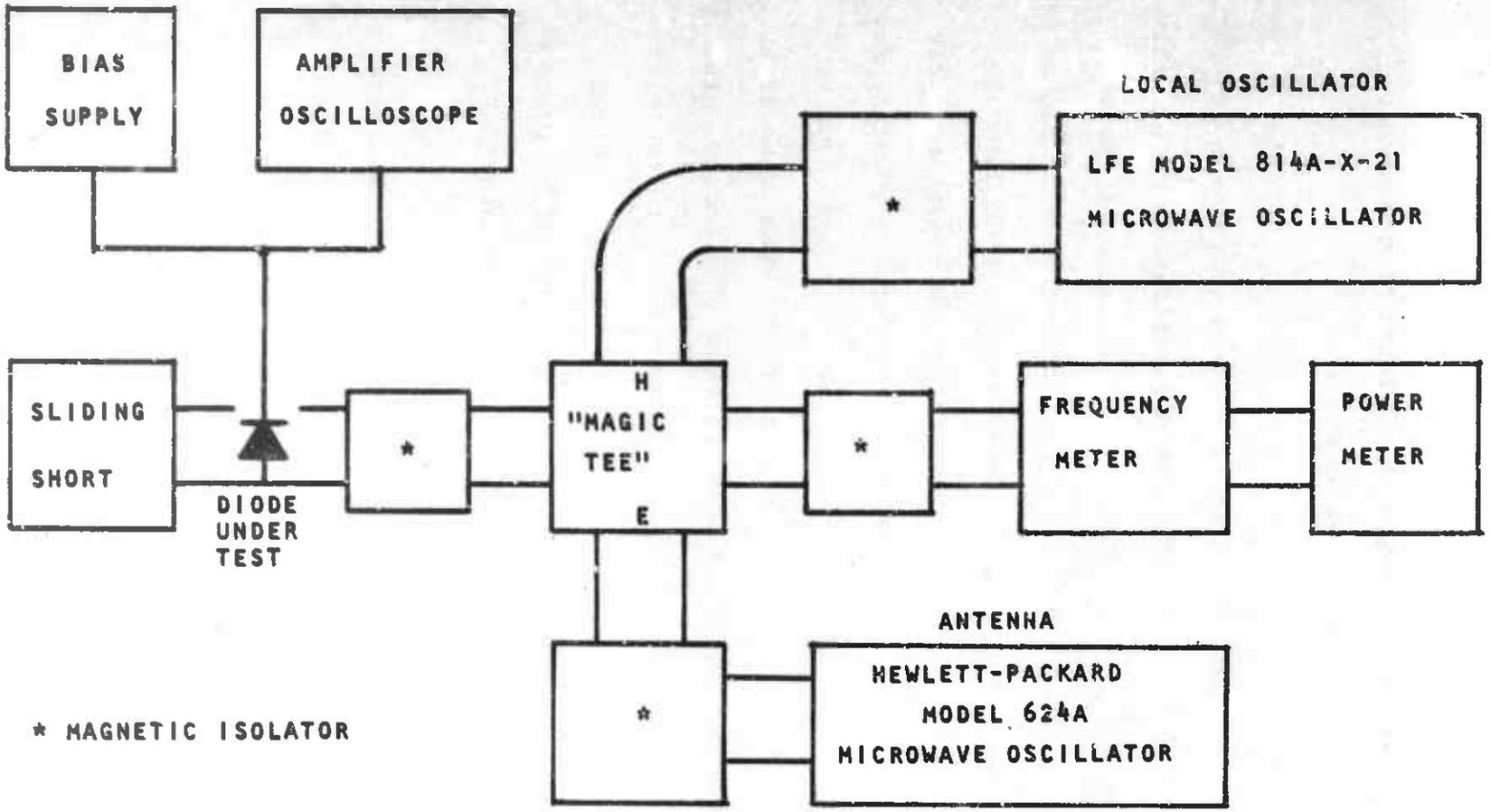

Figure 25. Circuit for Testing GaAs Schottky Barrier Diode as an X-band Mixer Diode

was checked before and after irradiation of the diodes. No change in noise figure was observed.

Before each X-ray pulse the antenna leg oscillator was adjusted between -45 dbm and -60 dbm to provide a 20×10^{-2} volt signal out of the I-F amplifier. The exact power setting was a function of the bias current applied to the diode under test. A typical output waveform is shown in figure 26. The change in maximum peak to peak amplitude as a function of bias current is shown in figure 27. An input of approximately 8×10^{-5} ampere is necessary to obtain an output from the amplifier of 1 volt.

The 30 MHz amplifier, because of its 8 MHz bandwidth, has a rise time of approximately 1.15×10^{-7} second. The output waveform (figure 26) is apparently the response of the amplifier to a narrow pulse that coincides with the X-ray pulse. This serves to illustrate one of the problems that will be encountered by receivers with narrow bandwidth I-F amplifiers in a radiation environment.

No changes were observed in any of the steady-state parameters of the diodes after irradiation. The noise figure remained constant. The V-I characteristics did not change. The diodes were exposed to a neutron gamma flux at the Sandia Pulsed Reactor II. Details are given in Appendix III.

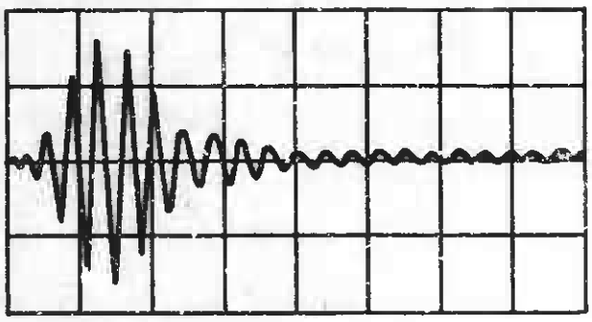

TIXV19-1
I_f=1 ma
Horizontal 100ns/cm
Vertical 200mv/cm

Figure 26. Response of GaAs Schottky Barrier Diode Operating as a Mixer Diode to an X-ray Pulse as Seen at the Output of the I-F Amplifier

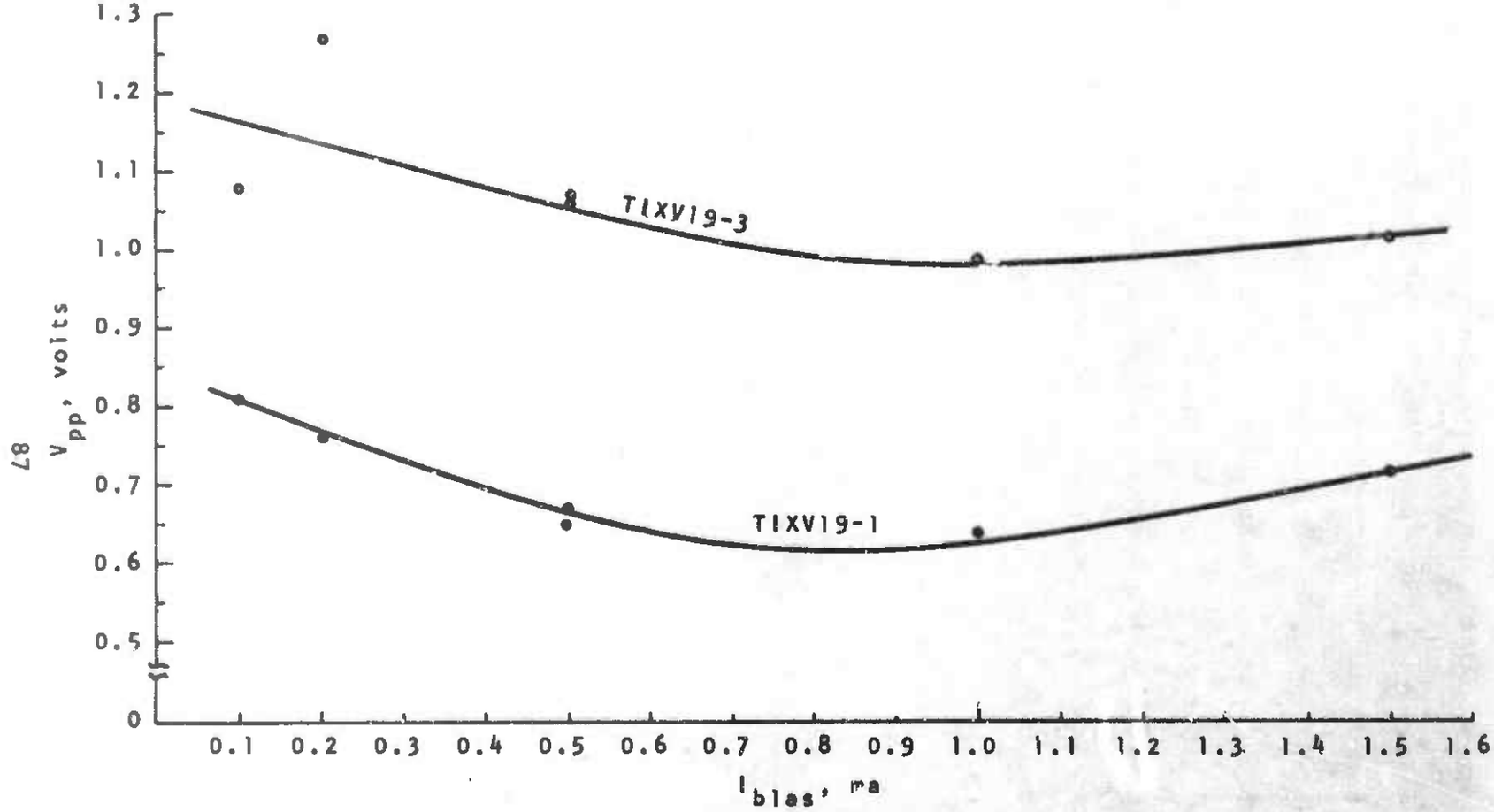

Figure 27. Maximum Peak to Peak Voltage versus Bias Current for TIXV19 X-band Mixer Diode

In summary, little can be said about the behavior of the Schottky barrier junction in a radiation environment. The response of the junction is masked by spurious response of the packaging and the surrounding environment.

This same limitation has been reached in experiments upon other types of devices. Further work can be done with larger junctions as they become available. In the long run, a more meaningful study would determine the sources of the spurious signals and develope techniques for their elimination.

APPENDIX I

DERIVATION OF VELOCITY DISTRIBUTION OF ELECTRONS FROM FERMI-DIRAC DISTRIBUTION

The velocity distribution of electrons can be developed from the Fermi-Dirac distribution function.

$$f(\mathcal{E}) = \frac{1}{\exp\left(\frac{E-E_f}{kT}\right) - 1} \qquad \text{(I-1)}$$

If we assume a nondegenerate semiconductor and we are interested in an arbitrary energy Δ above the conduction band, we can say

let

$$E = E_c + \Delta \qquad \text{(I-2)}$$

and

$$E_c + \Delta - E_f >> kT \qquad \text{(I-3)}$$

The Fermi-Dirac distribution function is now given by

$$f(E) = \exp\left[\frac{-(E_c - E_f + \Delta)}{kT}\right] \qquad (I\text{-}4)$$

If we assume a lightly doped semiconductor, then N_c, the density of quantum states in the conduction band, is greater than N_D, the concentration of donor atoms. N_c is given by

$$N_c = 2\left[\frac{2\pi m^* kT}{h^2}\right]^{3/2} \qquad (I\text{-}5)$$

The Fermi level in the semiconductor is given by

$$E_f = E_c - kT \ln \frac{N_c}{N_D} \qquad (I\text{-}6)$$

$$E_c - E_f = kT \ln \frac{N_c}{N_D} \qquad (I\text{-}7)$$

We now see that

$$f(E) = \exp(-\Delta/kT) \exp\left(-\ln \frac{N_c}{N_D}\right) \qquad (I\text{-}8)$$

$$f(E) = \frac{N_D}{N_c} \exp(-\Delta/kT) \qquad (I\text{-}9)$$

Substituting for N_c

$$f(E) = \frac{h^3}{2} (2\pi m^* kT)^{-3/2} N_D \exp(-A/kT) \qquad \text{(I-10)}$$

Digressing, we need to show that the density of states per unit volume in momentum space is $2/h^3$. Assuming a periodic lattice structure and a parabolic energy momentum relationship, we can state

$$E = \frac{p^2}{2m^*} = \frac{\hbar^2 k^2}{2m^*} \qquad \text{(I-11)}$$

where

$$p = \hbar k$$

and

$$\vec{k} = \frac{2\pi}{a} \vec{n}$$

where the vector $\vec{n}$ is defined by

$$\vec{n} = \vec{a}_x n_x + \vec{a}_y n_y + \vec{a}_z n_z \quad .$$

The quantities n_x, n_y, and n_z may assume both positive and negative integral values. Therefore equation I-11 becomes

$$E = \frac{\hbar^2 4\pi^2 n^2}{a^2 2m^*} \qquad \text{(I-12)}$$

A volume in n space is

$$V = 2 \cdot \frac{4}{3}\pi n^3 \qquad \text{(I-13)}$$

This volume is also Na^3, the number of states included within this spherical volume

$$N = \frac{8\pi}{3} \left(\frac{n}{a}\right)^3 \qquad \text{(I-14)}$$

It can be shown from the relations $k = \frac{2}{a} n$ and $p = \hbar k$ that

$$n^3 = \left(\frac{ap}{2\pi\hbar}\right)^3 \qquad \text{(I-15)}$$

Substituting equation I-15 into equation I-14, we get

$$N = \frac{8\pi p^3}{3h^3} \qquad \text{(I-16)}$$

$$dN = \frac{8\pi p^2}{h^3} dp \qquad \text{(I-17)}$$

Dividing by the volume of a spherical shell in p space and multiplying by a rectangular cartesian p-space volume element, we get

$$dN = \frac{2}{h^3} dp_x\, dp_y\, dp_z \qquad \text{(I-18)}$$

$$\frac{dN}{dp_x dp_y dp_z} = \frac{2}{h^3} \tag{I-19}$$

Now we can write the particle energy distribution per unit volume in momentum space as

$$\frac{f(E)\ 2}{h^3} = N_D(2\pi m^*\ kT)^{-3/2}\exp\ (-\Delta/kT) \tag{I-20}$$

Again assuming the parabolic energy momentum relationship, let

$$\Delta = \frac{p_x^2 + p_y^2 + p_z^2}{2m^*} \tag{I-21}$$

$$\frac{f(E)dN}{dp_x dp_y dp_z} = (2\pi m^* kT)^{-3/2}\ \exp\left(-\frac{p_x^2 + p_y^2 + p_z^2}{2m^* kT}\right) \tag{I-22}$$

Integrating over all $p_y + p_z$

$$\frac{f(E)dN}{dp_x} = (2\pi m^* kT)^{-1/2}\ \exp\left(\frac{-p_x^2}{2m^* kT}\right) \tag{I-23}$$

Changing variables from momentum to velocity, we get

$$f(E)dN = \left(\frac{m^*}{2\pi kT}\right)^{1/2} N_D \exp\left(-\frac{1}{2}\frac{m^*v_x^2}{kT}\right) dv_x \qquad (I\text{-}24)$$

This is the same as equation 14 in the text.

APPENDIX II

EXPERIMENTAL FACILITIES AND EQUIPMENT

All of the X-ray testing was done at Kirtland Air Force Base, Air Force Weapons Laboratory, with Air Force-supplied equipment. The X-ray source was a Field Emission Corporation Febetron Model 705. The Febetron is capable of producing a maximum X-ray dose of 3600 roentgens at dose rates up to 1.8×10^{11} r/sec. The X-ray pulse is triangular and approximately 17×10^{-9} second wide at the half peak intensity points.

The testing was done inside a double-walled copper screen room. Figure 28 shows a typical test configuration. All of the circuit except the diode under test is shielded from the X rays by at least 4 inches of lead. The viewing resistor was selected as 50 ohms to properly terminate the RG58 coaxial cable used throughout for signal transmission. Amplification or impedance matching was provided by Keithley Model 109 and Model 111 pulse amplifiers, which have 20 db and 0 db voltage gain, respectively.

A Tektronix Model 517 oscilloscope was used in conjunction with a Model C19 camera to record all transient signals. A variable attenuator was used at the oscilloscope to provide gain control and impedance matching.

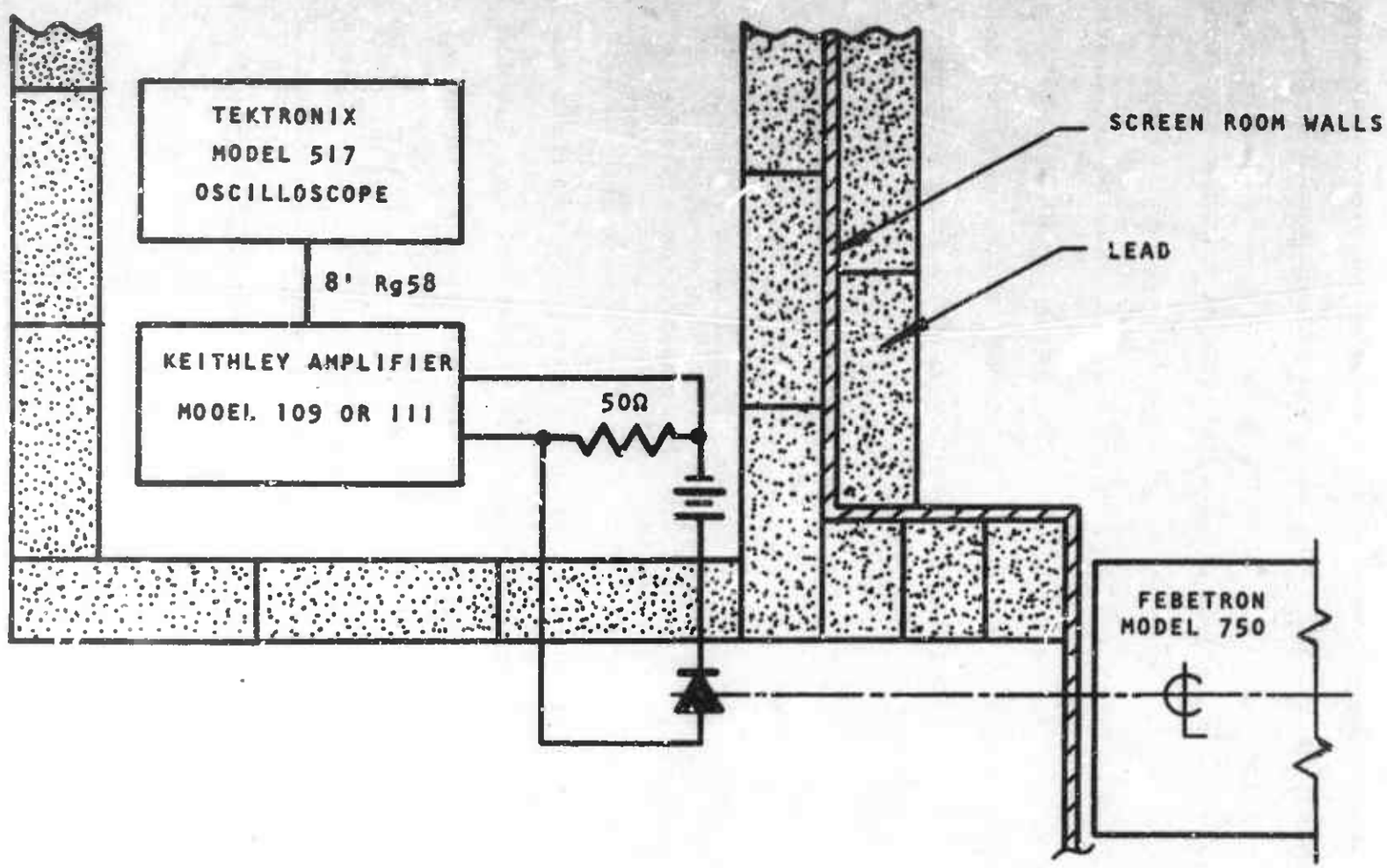

Figure 28. Typical Test Configuration Showing Screen Room and Flash X-ray Machine

Inside the screen room, at a distance of approximately 8 inches from the wall, the dose received by the diode under test was approximately 20 rads. Other dose levels were obtained by changing the position of the diode.

APPENDIX III

RESULTS OF NEUTRON TESTING OF SCHOTTKY BARRIER DIODES

The effect of neutron bombardment upon Schottky barrier diodes was investigated. The diodes were tested at the Sandia Pulsed Reactor (SPR) II. The SPR II is capable of producing a neutron fluence of 5×10^{13} nvt and a gamma dose rate of 10^{9} R/sec at its outside surface. A fluence of 5×10^{14} nvt can be obtained by positioning the components under test inside the "glory hole." The glory hole is a 1.5-inch-diameter hole that extends into the center of the reactor.

Five of the TIV19 GaAs Schottky barrier diodes and five of the TIV305 silicon Schottky barrier diodes were tested. The diodes were exposed to a total fluence ranging from 9.2×10^{13} to 1.2×10^{15} nvt.

The original test configuration was designed to monitor transient annealing of the diodes. No transient annealing was observed. The gamma burst dominated the response for at least 10^{-2} second after each burst. After more time had elapsed, the diode was found to be undamaged.

The remainder of the tests were performed without real time measurements. The tests consisted of measuring

the current voltage characteristics of the diodes before and after irradiation. The current was measured over a range of 10^{-7} to 10^{-2} ampere.

The test results for the TIXV19-7 GaAs Schottky barrier diode are shown in figure 29. The curve labeled 0 gives the V-I characteristic before irradiation. Curve 1 is the characteristic after the first burst, with fluence of 9.76×10^{13} nvt. Curves 2, 3, and 4 are the V-I characteristics after the second, third, and fourth bursts, with fluences of 1.12×10^{14}, 4.5×10^{14}, and 4.92×10^{14} nvt, respectively.

The curves shown in figure 29 were not called typical because the change of the TIXV19 characteristic was not consistent from diode to diode nor from burst to burst. The slope of the V-I usually increased; however, this was not always the case. The slope for the TIXV19-7 increased for all bursts except burst 3.

The following generalizations can be made about the TIXV19 GaAs Schottky barrier diode exposed to a fluence of 10^{15} nvt or less:

1. The forward V-I characteristics do not change for currents larger than 10^{-4} ampere.
2. The forward V-I characteristics show a lower resistance for currents less than 10^{-4} ampere.
3. The diode reverse leakage current increases slightly.

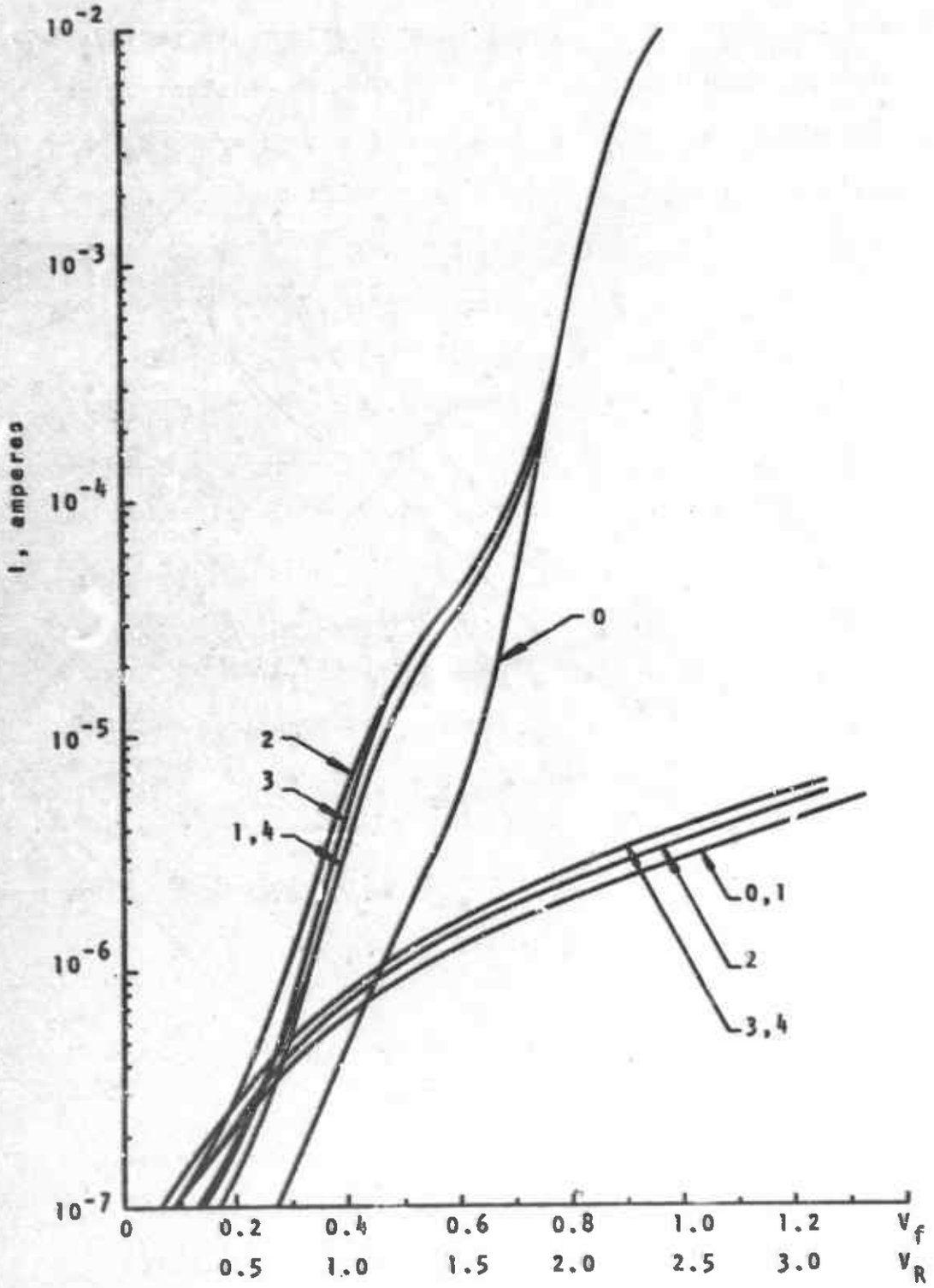

Figure 29. TIXV19-7 V-I Characteristics Before and After Exposure to Neutrons

The changes in the TIXV19 GaAs Schottky barrier diode are not sufficient to significantly affect its performance in a practical circuit. The level at which significant degradation of the diode occurs was not determined. A neutron fluence greater than that available at SPR II is necessary for this determination.

Similar but more erratic results were observed from tests of the TIV305 silicon Schottky barrier diodes. Figure 30 shows the V-I characteristics of the TIV305-5 diode before and after irradiation. Curve 0 is before irradiation. Curve 1 is after the first burst, which had a fluence of 1.12×10^{14} nvt, and curve 2 is after the second burst which had a fluence of 4.92×10^{14} nvt.

Further tests with fluences greater than 10^{15} nvt should be performed in order to determine the tolerance level of Schottky barrier diodes. Because of the non-uniform behavior of the diodes, a large number of each type of diode should be tested so that statistical data may be obtained.

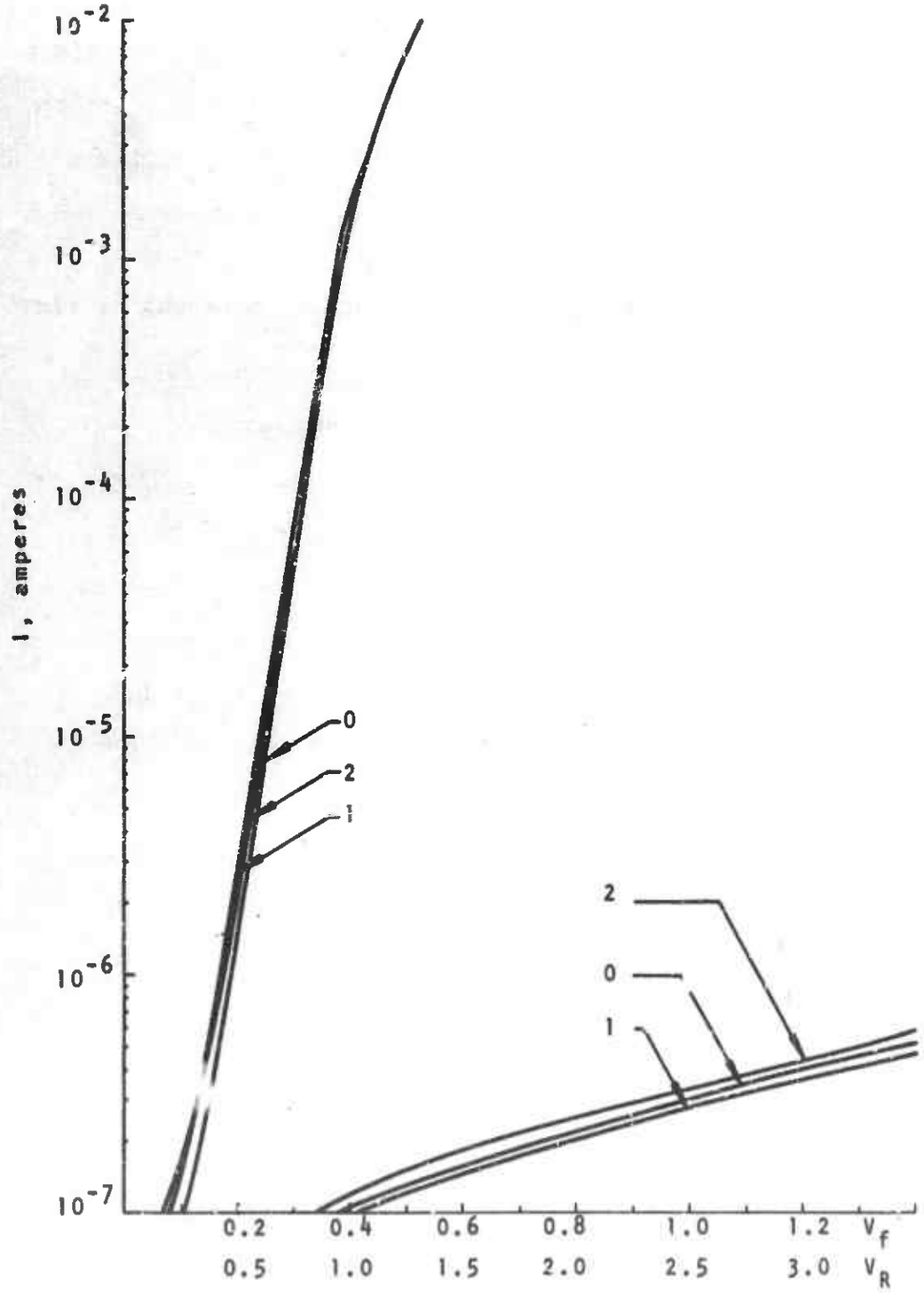

Figure 30. TIV305-5 V-I Characteristics Before and After Exposure to Neutrons

REFERENCES

1. Henish, H. K., Rectifying Semiconductor Contacts, Oxford University Press, Oxford, 1957.

2. Van der Ziel, A., Solid State Electronics, Prentice-Hall, Inc., Englewood Cliffs, 1957.

3. Moll, J., Physics of Semiconductors, McGraw-Hill Book Company, Inc., New York, 1964.

4. Kingston, R. H., and Neustadter, S. F., "Calculation of Space Charge, Electric Field, and Free Carrier Concentration at the Surface of a Semiconductor," J. Appl. Phys., Vol. 26, pp. 718-720, June 1955.

5. Schwartz, R. F., and Walsh, J. F., "The Properties of Metal to Semiconductor Contacts," IRE Proc., pp. 1715-1720, December 1953.

6. Seiwatz, R., and Green, M., "Space Charge Calculations for Semiconductors," J. App. Phys., Vol. 29, pp. 1034-1040, July 1958.

7. Cowley, A. M., Surface States and Barrier Height in Metal-Semiconductor Surface Barrier Diodes, Stanford Electronics Laboratories, Stanford, 1965.

8. Crowell, C. R., "Quantum-Mechanical Reflection of Electrons at Metal-Semiconductor Barriers: Electron Transport in Semiconductor-Metal-Semiconductor Systems," J. App. Phys., Vol. 37, pp. 2683-2689, June 1966.

9. Crowell, C. R., and Sze, S. M., "Current Transport in Metal-Semiconductor Barriers," Solid State Electronics, Vol. 9, pp. 1035-1048, 1966.

10. Padovani, F. A., and Stratton, R., "Field and Thermionic Emission in Schottky Barriers," Solid State Electronics, Vol. 9, pp. 695-707, 1966.

11. Goodman, A. M., "Metal-Semiconductor Barrier Height Measurement by the Differential Capacitance Method--One Carrier System," J. App. Phys., Vol. 34, pp. 329-338, February 1963.

References, Cont.

12. Bardeen, J., "Surface States and Rectification at a Metal Semiconductor Contact," Phys. Review, Vol. 71, pp. 717-727, May 1947.

13. Cowley, A. M., and Sze, S. M., "Surface States and Barrier Height of Metal-Semiconductor Systems," J. App. Phys., Vol. 36, pp. 3212-3220, October 1965.

14. Mead, C. A., "Metal-Semiconductor Surface Barriers," Solid State Electronics, Vol. 9, pp. 1023-1033, 1966.

15. Grimley, T. B., "Surface States Associated with Adsorbed Atoms," J. Phys. Chem. Solids, Vol. 14, pp. 227-232, 1960.

16. Shockley, W., "On the Surface States Associated with a Periodic Potential," Phys. Review, Vol. 56, pp. 317-323, August 1939.

17. Mead, C. A., and Spitzer, W. G., "Fermi Level Position at Metal-Semiconductor Interfaces," Phys. Review, Vol. 134, pp. A713-A716, May 1964.

18. Scharfetter, D. L., "Minority Carrier Injection and Charge Storage in Epitaxial Schottky Barrier Diodes," Solid State Electronics, Vol. 8, pp. 299-311, 1965.

19. Van Lint, V. A. J., et al., The Effect of Pulsed Gamma Radiation on Dynamic Electronic Components, GA-4062, General Atomics, San Diego, 1964.

20. Hall, R. N., "Electron-Hole Recombination in Germanium," Phys. Review, Vol. 87, p. 387, 1962.

21. Shockley, W., and Read, W. T., "Statistics of the Recombination of Holes and Electrons," Phys. Review, Vol. 87, pp. 835-842, September 1952.

22. Wirth, J., and Rodgers, S., The Transient Response of Transistors and Diodes to Ionizing Radiation, Sandia Corp., Report No. SC-R-64-194, Albuquerque, 1964.

23. Wilson, D. K., et al., Effects of Radiation on Semiconductor Materials and Devices, AFCRL-67-0068, Bell Laboratories, New York, 1966.

24. Padovani, F., and Summer, G., "Experimental Study of Au GaAs Schottky Barriers," J. App. Phys., Vol. 36, pp. 3744-3747, December 1965.

References, Cont.

25. Kahng, D., "Au-N-Type GaAs Schottky Barrier and its Varactor Application," Bell System Technical J., pp. 215-224, January 1964.

26. Kahng, D., "Conduction Properties of the Au-n-Type-Si Schottky Barrier," Solid State Electronics, Vol. 6, pp. 281-295, 1963.

27. Sze, S. M., Crowell, C. R., and Kahng, D., "Photoelectric Determination of the Image Force Dielectric Constant for Hot Electrons in Schottky Barriers," J. App. Phys., Vol. 35, pp. 2534-2536, August 1964.

28. Ashley, K. L., and Baird, J. R., Optical Microprobe Response of GaAs Diodes, Texas Instruments Inc., SC0734, October 1966.

BIBLIOGRAPHY

Aukerman, L. W., "Annealing of Electron-Irridiated GaAs," Phys. Review, Vol. 127, pp. 1576-1583, September 1962.

Aukerman, L. W., "Radiation Effects in GaAs," J. App. Phys., Vol. 34, pp. 3590-3599, December 1963.

Denker, S. P., and Scarengella, D., "Competing Detection Mechanisms in Hot Carrier Microwave Diodes," Solid State Electronics, Vol. 10, pp. 777-789, 1967.

Dienes, G. J., and Vineyard, G. H., Radiation Effects in Solids, Interscience Publishers, Inc., New York, 1957.

Eisen, F. H., "Radiation Damage in Semiconducting III-V Compounds," Radiation Damage in Semiconductors, Paris-Royaumont, pp. 163-171, 1964.

Gossick, B. R., Potential Barriers in Semiconductors, Academic Press, New York, 1964.

Gossick, B. R., "Metal-Semiconductor Rectifiers and Transistors," Solid State Electronics, Vol. 6, pp. 445-452, 1963.

Gossick, B. R., "On the Transient Behavior of Semiconductor Rectifiers," J. App. Phys., Vol. 27, pp. 905-911, August 1956.

Grimshaw, J. A., "Effects of Electron Irradiation on the Mobility of Electrons in Gallium Arsenide," Radiation Damage in Semiconductors, Paris-Royaumont, pp. 377-383, 1964.

Hilsum, C., and Rose-Innes, A. C., Semiconducting III-V Compounds, Pergamon Press, New York, 1961.

Hine, G. J., and Brownell, G. L., Radiation Dosimetry, Academic Press, New York, 1956.

Landsberg, P. T., "The Theory of Direct-Current Characteristics of Rectifiers," Proc. Roy. Soc., Vol. A206, pp. 463-476, 1951.

Landsberg, P. T., "Contributions to the Theory of Heterogeneous Barrier Layer Rectifiers," Proc. Roy. Soc., Vol. A206, pp. 477-488, 1951.

Loferski, J. J., and Wu, M. H., "Studies of Radiation Defects in GaAs Based upon Proton--and Electron--Bombardment Induced Light Emission," Radiation Damage in Semiconductors, Paris-Royaumont, pp. 213-217, 1964.

MacDonald, J. R., "Accurate Solution of an Idealized One-Carrier Metal-Semiconductor Junction Problem," Solid State Electronics, Vol. 5, pp. 11-37, 1962.

Madelung, O., Physics of III-V Compounds, John Wiley & Sons, Inc., New York, 1964.

Many, A., Goldstein, Y., and Grover, N. B., Semiconductor Surfaces, North-Holland Publishing Company, Amsterdam, 1965.

Mayberg, S., "Direct Recombination in GaAs and Some Consequences in Transistor Design," Solid State Electronics, Vol. 2, pp. 195-201, 1961.

Nanavati, R. P., An Introduction to Semiconductor Electronics, McGraw-Hill Book Company, Inc., New York, 1963.

Shockley, W., Electrons and Holes in Semiconductors, D. Van Nostrand Company, Inc., Princeton, 1950.

Spenke, E., Electronic Semiconductors, McGraw-Hill Book Company, Inc., New York, 1958.

Stratton, R., "Diffusion of Hot and Cold Electrons in Semiconductor Barriers," Phys. Review, Vol. 126, pp. 2002-2014, 1962.

Strettan, J. S., Ionizing Radiations, Pergamon Press, Oxford, 1965.

Vavilov, V. S., Effects of Radiation on Semiconductors, Consultants Bureau, New York, 1965.

UNCLASSIFIED
Security Classification

DOCUMENT CONTROL DATA - R & D

(Security classification of title, body of abstract and indexing annotation must be entered when the overall report is classified)

1. ORIGINATING ACTIVITY (Corporate author)
University of New Mexico
Albuquerque, New Mexico

2a. REPORT SECURITY CLASSIFICATION
Unclassified

2b. GROUP

3. REPORT TITLE
RADIATION EFFECTS ON GALLIUM ARSENIDE DEVICES AND SCHOTTKY DIODES
Volume I

4. DESCRIPTIVE NOTES (Type of report and inclusive dates)
15 February 1967 to 15 February 1968

5. AUTHOR(S) (First name, middle initial, last name)
R.H.Schnurr
H. D. Southward

6. REPORT DATE	7a. TOTAL NO. OF PAGES	7b. NO. OF REFS
August 1968	128	28

8a. CONTRACT OR GRANT NO.	9a. ORIGINATOR'S REPORT NUMBER(S)
F29601-67-C-0051	
b. PROJECT NO. 5710	AFWL-TR-68-31, Vol I
c. Subtask No. 6.015	9b. OTHER REPORT NO(S) (Any other numbers that may be assigned this report)
d.	

10. DISTRIBUTION STATEMENT This document is subject to special export controls and each transmittal to foreign governments or foreign nationals may be made only with prior approval of AFWL (WLRET), Kirtland AFB, NMex 87117. Distribution is limited because of the technology discussed in the report.

11. SUPPLEMENTARY NOTES	12. SPONSORING MILITARY ACTIVITY
	AFWL (WLRET) Kirtland AFB, NMex 87117

13. ABSTRACT

(Distribution Limitation Statement No. 2)

The theory of operation of the Schottky barrier diode is reviewed, and complications caused by a more accurate space-charge formulation are discussed. Consideration is given to image effects, tunneling, interfacial dielectric layers, surface states, and minority carrier current.

The interaction of ionizing radiation with semiconducting materials is reviewed, as is the behavior of a Schottky barrier diode in an ionizing radiation environment. The resultant model for the Schottky barrier diode is analogous to a p-n diode with a very high dopant concentration on one side.

Tests were performed upon gallium arsenide (GaAs) and silicon Schottky barrier diodes using a 2-Mev flash X-ray machine. The GaAs Schottky diodes were tested while functioning as an X-band detector and mixer. No permanent change was observed in the voltage-current or capacitance-voltage characteristics, or in the noise figure of the diodes after irradiation. Diodes fabricated from both types of material were also tested in a more conventional DC bias circuit.

Both types of diode were exposed to a mixed neutron gamma pulse at the Sandia Pulsed Reactor II. Neutron fluences up to 5×10^{14} nvt and gamma dose rates up to 10^9 rad/sec were obtained. The diodes showed very minor changes in voltage current characteristics for a total neutron fluence up to 1.2×10^{15} nvt.

DD FORM 1 NOV 65 1473

UNCLASSIFIED
Security Classification

14. KEY WORDS	LINK A		LINK B		LINK C	
	ROLE	WT	ROLE	WT	ROLE	WT
Radiation effects on electronics						
Schottky barrier diodes, radiation effects on						
Gallium Arsenide Semiconductors, radiation effects on						